Horizon 2020 Programme

METIS

Research and Innovation Action (RIA)

This project has received funding from the European Union's Horizon 2020 research and innovation programme under grant agreement No 945121

Start date : 2020-09-01 Duration : 57 Months

Fragility curves for METIS case study

Authors : Mohamed ZOUATINE (TUK)

METIS - Contract Number: 945121

Project officer: Katerina PTACKOVA

Document title	Fragility curves for METIS case study
Author(s)	Mohamed ZOUATINE
Number of pages	49
Document type	Deliverable
Work Package	WP6
Document number	D6.8
Issued by	TUK
Date of completion	2025-05-28 22:39:17
Dissemination level	Public

Summary

In this report, we present a detailed fragility analysis of the chosen structures, systems, and components (SSCs) of the Zaporizhzhia Nuclear Power Plant (NPP). A total of six finite element (FE) models were developed: Reactor Building (RB), Diesel Generator Building (DGB), Filter Containment Venting System (FCVs), Transformer, Control Monitor Cabinet (CMC), and Service Water Pump (SWP), as identified in Task 6.1. These models utilized advanced FE techniques, including multilayer shell elements to capture shear wall behavior and fibre-based methods for piping response. Nonlinear behavior was modelled using Popovics material for concrete, and the OpenSees open-source software was used to construct and validate these models with real data from the Zaporizhzhia NPP and other relevant NPP reports. To incorporate soil-structure interaction (SSI), the models were enhanced with spring elements, capturing key SSI parameters such as stiffness and damping. For the fragility analysis, the cloud-regression method was chosen, enabling parameter estimation (median and dispersion) of fragility curves based on responses from nonlinear dynamic simulations without the need for ground motion scaling. This method aligns with previous work packages (e.g., WP5 on ground motion development) and is particularly suited for NPP structures, which are designed to remain largely linear under seismic events, because the used fragility method enables the estimation of failure probabilities even when no or limited failure data is available. Throughout this task, uncertainty propagation was integrated, with key uncertainties integrated from the source, through soil characteristics, and into structural responses. Soil parameter uncertainties were incorporated through the spring methodology, while material and damping uncertainties were included in the numerical models. For the threshold definition, the failure in the structures (Reactor Building, Diesel Generator Building) was defined as the exceedance of the compressive strength of the concrete. The failure of the remaining components, however, is determined based on their respective failure mechanisms. The engineering demand parameter (EDP) was selected to be the drift in terms of structure and displacement in terms of components, the intensity measure (IM) was selected to be peak ground acceleration (PGA). For the specified threshold, the fragility analysis indicates the NPP-structure, namely the Reactor Building and Diesel Generator Bu...

Approval

Date	By
2025-05-28 22:46:04	Mohamed ZOUATINE (TUK)
2025-05-28 22:53:21	Irmela ZENTNER (EDF)

METIS

Seismic Risk Assessment for Nuclear Safety

Research & Innovation Action

NFRP-2019-2020

Fragility computations for METIS case study

Deliverable D6.8

Version N°3

Authors:

Mohamed Zouatine M.Sc. (RPTU)

Dr. Irmela Zentner (EDF)

Prof. Dr.-Ing. Hamid Sadegh-Azar (RPTU)

Disclaimer

The content of this deliverable reflects only the author's view. The European Commission is not responsible for any use that may be made of the information it contains.

Document Information

Grant agreement	945121
Project title	Methods And Tools Innovations For Seismic Risk Assessment
Project acronym	METIS
Project coordinator	Dr. Irmela Zentner, EDF
Project duration	1st September 2020 – 31st May 2025 (57 months)
Related work package	WP 6 – Beyond Design and Fragility Analysis
Related task(s)	Task 6.8 – Fragility computations for METIS case study
Lead organisation	TUK
Contributing partner(s)	TUK
Due date	31st May 2025
Submission date	28/05/2025
Dissemination level	Public

History

Version	Submitted by	Reviewed by	Date	Comments
N°1	Mohamed Zouatine	John Richards	21/01/2025	
N°2	Mohamed Zouatine	Dmytro Ryzhov	26/02/2025	
N°3	Mohamed Zouatine	Tadeusz Szczesiak	20/05/2025	

Table of Contents

List of figures

List of tables

Abbreviations and Acronyms

Acronym	Description
NPP	Nuclear Power Plant
SSC	System, Structure, Component
FEM	Finite Element Model
SSI	Soil Structure Interaction
RB	Reactor Building
DGB	Diesel Generator Building
FCVs	Filter Containment Venting System
CMC	Control Monitor Cabinet
SWP	Service Water Pump
LHS	Latin Hypercube Sampling
IM	Intensity Measure
PGA	Peak Ground Acceleration
EDP	Engineering Demand Parameter
BE	Best Estimate
BEU	Best Estimate and Uncertainties
GeoMean	Geometric Mean
FEMA	Federal Emergency Management Agency
EPRI	Electric Power Research Institute
HCLPF	High Confidence Low Probability of Failure
IDA	Incremental Dynamic Analysis
MSA	Multiple Stripe Analysis

Summary

In this report, we present a detailed fragility analysis of the chosen structures, systems, and components (SSCs) of the Zaporizhzhia Nuclear Power Plant (NPP). A total of six finite element (FE) models were developed: Reactor Building (RB), Diesel Generator Building (DGB), Filter Containment Venting System (FCVs), Transformer, Control Monitor Cabinet (CMC), and Service Water Pump (SWP), as identified in Task 6.1. These models utilized advanced FE techniques, including multilayer shell elements to capture shear wall behavior and fibre-based methods for piping response. Nonlinear behavior was modelled using Popovics material for concrete, and the OpenSees open-source software was used to construct and validate these models with real data from the Zaporizhzhia NPP and other relevant NPP reports.

To incorporate soil-structure interaction (SSI), the models were enhanced with spring elements, capturing key SSI parameters such as stiffness and damping. For the fragility analysis, the cloud-regression method was chosen, enabling parameter estimation (median and dispersion) of fragility curves based on responses from nonlinear dynamic simulations without the need for ground motion scaling. This method aligns with previous work packages (e.g., WP5 on ground motion development) and is particularly suited for NPP structures, which are designed to remain largely linear under seismic events, because the used fragility method enables the estimation of failure probabilities even when no or limited failure data is available.

Throughout this task, uncertainty propagation was integrated, with key uncertainties integrated from the source, through soil characteristics, and into structural responses. Soil parameter uncertainties were incorporated through the spring methodology, while material and damping uncertainties were included in the numerical models.

For the threshold definition, the failure in the structures (Reactor Building, Diesel Generator Building) was defined as the exceedance of the compressive strength of the concrete. The failure of the remaining components, however, is determined based on their respective failure mechanisms. The engineering demand parameter (EDP) was selected to be the drift in terms of structure and displacement in terms of components, the intensity measure (IM) was selected to be peak ground acceleration (PGA).

For the specified threshold, the fragility analysis indicates the NPP-structure, namely the Reactor Building and Diesel Generator Building, exhibit high median capacity values with moderate dispersion. In contrast, components and systems display low to moderate median capacities. The highest dispersion is observed in the Filter Containment Venting System (FCVs) model, primarily due to its multi-support configuration across various elevations of the Reactor Building, which introduces significant variability to the system's response.

Keywords

Fragility analysis, structure, system, components, uncertainty propagation, finite element modelling, soil structure interaction, Engineering Demand Parameter, intensity measure.

Introduction

The objective of Deliverable D6.8, titled "Fragility computations for METIS Case Study," is to evaluate the performance of selected nuclear power plant (NPP) structural system components (SSCs) subjected to seismic ground motions provided by WP5. This performance assessment is presented through fragility curves, which represent the probability of SSCs failure under specified ground motion intensities.

Data for modelling the SSCs were sourced from a real case study at the Zaporizhzhia NPP. Where additional information on certain SSCs was required, supplementary data from reports, such as those by EPRI and other relevant reports, were utilized to ensure detailed and accurate modelling. The developed models were validated based on the dynamic characteristics and nonlinear performance of the SSCs provided in these reports. Soil-structure interaction (SSI) effects were also incorporated by modelling springs and dashpots with input values reflecting the local soil conditions for the structures. To account for uncertainties in the structural and component responses, findings from Deliverable 6.4 were applied. These findings demonstrated that the Latin Hypercube method provides reliable results compared to other rigorous approaches, making it the chosen method for fragility analysis.

The current state of the art offers a variety of methodologies for performing fragility analysis. Some of these are numerical simulation-based, including Cloud Analysis, Incremental Dynamic Analysis (IDA), Multiple Stripe Analysis (MSA), Bayesian Updating, and factor combination-based methodologies, such as the Method of Separation of Variables (SOV) (EPRI Approach). In the context of seismic fragility assessment of nuclear power plant (NPP) structures, the SOV method is the prevailing approach. This method estimates fragility parameters by accounting for various capacity-related factors, such as strength and inelastic energy absorption, as well as demand and response parameters, including spectral shape, soil-structure interaction, and modal combinations. A key advantage of the SOV method is its efficiency in developing fragility curves without the computational expense associated with numerical simulation-based approaches. However, it is important to acknowledge that the SOV method assumes linear relationships between these parameters. In contrast, numerical simulation methods address this limitation by capturing nonlinear effects and enabling the propagation of uncertainties throughout the model. For this task, the cloud-regression methodology was chosen as it was found to be the most suitable for NPP facilities applications. This method is particularly advantageous as it allows for the estimation of failure probability even when no failure is observed from nonlinear dynamic analysis (NLDA).

The report is organized into four sections. Section 1 outlines the methodology used to develop numerical models for the selected SSCs, as specified in Task 6.1, including structural data (architectural drawings, material properties) and the finite element approaches applied. It also presents the validation of these models using real data from the Zaporizhzhia NPP. Section 2 details the ground motions used to develop the fragility curve. Section 3 describes the fragility analysis method, the SSI approach employed, and the specific uncertainties considered in structural modelling. It also presents the fragility results, including the median capacity and dispersion of the analysed components. The final section, Section 4, discusses and evaluates the outcomes of the work, leading to a conclusion based on the findings.

1 Overview of SSCs and Finite Element Models

1.1 General Description

Nuclear power plants (NPPs) are considered highly sensitive structures due to the significant risks associated with the failure of their components. In addition to their critical importance, NPPs are among the most complex structures to assess risks related to seismic activity. This complexity arises from the need to ensure the integrity of various structures, systems, and components that must function correctly throughout the plant's design life.

The structure of an (NPP) includes numerous components, all of which must operate reliably over the plant's lifetime. These components include, but are not limited to Auxiliary Building, Turbine Building, Pump House, 400kV/27kV transformers, 10kV switchgear, 200V DC cabinets, solenoid valves, shutdown panels, storage tanks, heat exchangers, filter containment systems, and motor-operated valves. These components are typically housed in critical areas of the NPP, such as the Diesel Generator Building or the Reactor Building, to ensure their proper functioning and safety during operation [1].

One of the key steps in conducting a risk assessment is calculating the probability of structural failure due to an induced hazard, such as an earthquake. This process is known as fragility analysis [2]. Given the complexity and critical importance of the structures within a nuclear power plant (NPP), selecting the most critical components for seismic risk assessment can be particularly challenging. However, despite these challenges, it is possible to select Structures, Systems, and Components (SSCs) based on specific criteria that prioritize those most critical to the plant's safety and operational integrity. These criteria might include the components' roles in ensuring the plant's safe shutdown, their impact on preventing radioactive releases, or their importance in maintaining the overall functionality of the NPP during and after a seismic event.

Following these criteria, the relevant Structures, Systems, and Components (SSCs) were selected for their critical roles in the functioning of the nuclear power plant. These SSCs include the Reactor Building (RB), Diesel Generator Building (DGB), Filter Containment System (FCVs), Transformer, Control Monitor Cabinet (CMC), and Service Water Pump (SWP). Each of these components plays a vital role in the safe and efficient operation of the NPP (more details on main contributors to risk for METIS cases study can be found in deliverable METIS D6.1 [3]):

1- **Reactor Building (RB)**: As the containment structure for the nuclear reactor, the Reactor Building is essential for housing the reactor core and protecting against the release of radioactive materials. It also provides physical protection to the reactor from external hazards.

2- **Diesel Generator Building (DGB)**: The Diesel Generator Building houses the backup power supply systems. In the event of a power outage, the diesel generators ensure that critical systems, including cooling systems and safety mechanisms, continue to function, preventing a potential meltdown.

3- **Filter Containment Venting System (FCVs)**: is used to prevent overpressure in the reactor's security containment. It primarily consists of a dirty gas pipe, a Venturi scrubber, and a clean gas pipe. The dirty gas pipe carries gases from the reactor containment, passing over buildings like CD and the Machine House 2F/3F, leading to the venting building ZX. Along this path, the pipes are supported by various structural supports attached to different buildings.

4- **Transformer 6kV-380V**: The transformer is responsible for converting the electrical output from the reactor to a suitable voltage level for distribution. It plays a key role in the power

generation process and in maintaining the electrical stability of the plant. The 6kV-380V transformers are oil-filled units with 800 kVA electrical power ratings. They are anchored by clamps. The weight of each transformer is 2420 kg.

5- **Control Monitor Cabinet (CMC)**: The Control Monitor Cabinet houses the essential control and monitoring systems that manage the reactor's operation. It allows operators to monitor reactor conditions in real time and to take necessary actions to ensure safe operation. The cabinet is anchored to the floor via expansion anchors that secure angles to the floor and are bolted to the cabinet base.

6- **Service Water Pump (SWP)**: The Service Water Pump is essential for providing cooling water to various systems within the NPP, including the reactor and auxiliary systems. It ensures that these systems do not overheat, which is vital for maintaining the plant's safety and operational efficiency.

As far as Zaporizhzhia NPP is concerned, the characteristics of the selected SSCs (including geometry, materials, etc.) were based on the specifics of the Zaporizhzhia NPP. However, due to the sensitivity of the documents, which are confidential, it was challenging to obtain all the necessary information for modelling purposes. To address this challenge, supplementary information was sourced from other documents, such as those from the Electric Power Research Institute (EPRI) and documentation from other nuclear power plants, to fill the gaps in data.

Some of the selected SSCs are located in both the Diesel Generator Building and the Reactor Building such the transformer. Table 1.1 provides detailed information about the location and position of these selected SSCs at Zaporizhzhia NPP:

Table 1.1 Location of the Selected SSCs at Zaporizhzhia Nuclear Power Plant (NPP)

Reactor Building		**Diesel Generator Building**	
SSCs	**Elevation**	**SSCs**	**Elevation**
FC Venting System	Supported at different elevation	**Transformer 6kV-380V**	0
Transformer 6kV-380V	20.4	**Service Water Pump**	-7
Control Monitor Cabinet	13.2		

Following the introduction to the selection of SSCs, the next section will offer a detailed description of the properties of the selected SSCs, the modelling approach used to develop the mathematical model, capturing the nonlinear behavior and the validation of the developed models.

1.2 Structural Characteristics and Finite Element Modelling of NPP Structures

1.2.1 Reactor Building

The reactor building at the Zaporizhzhia NPP is composed of three primary sections: the outer building, the containment structure supported by a common foundation (Figure 1.1). Most key components, such as the reactor internals, are housed within the containment structure. This containment ensures the reactor is isolated from the environment and, in the event of potential accidents, confines radioactive substances within it.

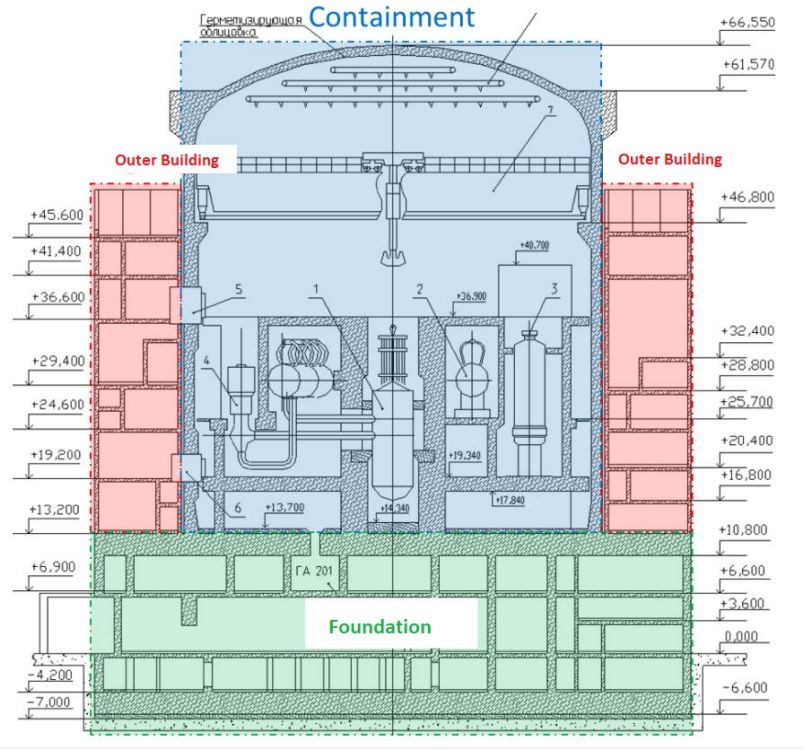

Figure 1.1 Reactor Building

The containment is positioned on a foundation at a height of 13.2 meters to supply and unload the active and spent nuclear fuel from the transport corridor to level 0 through the containment bottom containment hatch. The cylindrical section of the containment is prestressed with each tendon consisting of 456 high strength wires 5 mm in diameter. The cylindrical part has 96 tendons, and the dome part has 36 tendons. The cylindrical section has a diameter of 45 meters (Figure 1.2) and a total height of 53.35 meters, covered with a spherical dome. The thickness of the containment cylindrical part is 1.2 m, and the containment dome part is 1.1 m.

The outer structure encloses the containment on a common foundation set at an elevation of 13.20 meters. This structure is a multi-story rectangular design, incorporating stairwells and elevator shafts at its corners. The foundation is a rectangular reinforced concrete structure with plan dimensions of 66 x 66 meters (Figure 1.2) and a height of 20 meters, extending from the base level at -7.2 meters to the top at 13.2 meters. It is important to note that the foundation serves as the only connection between the outer building and the containment parts.

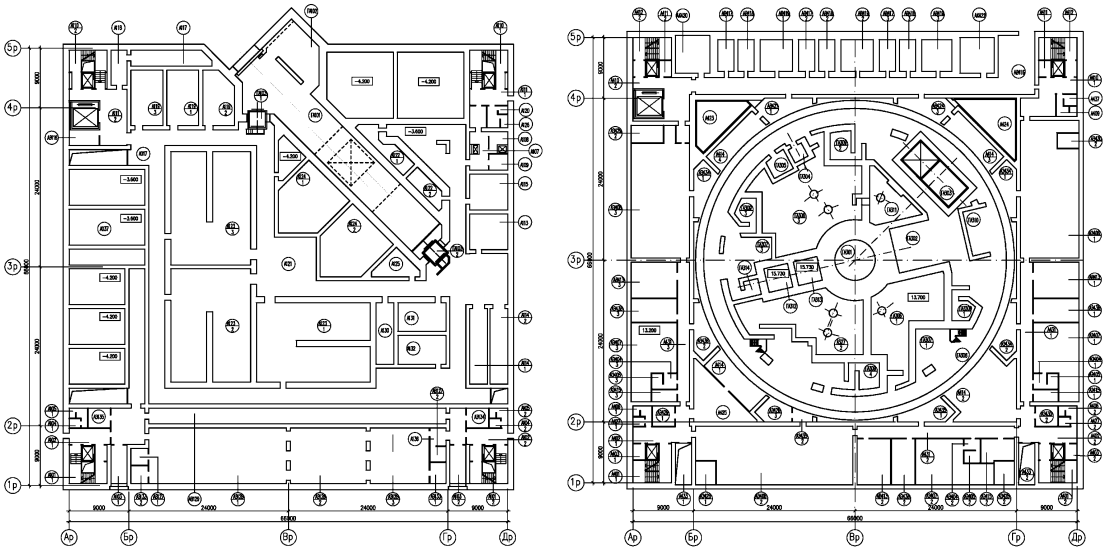

Figure 1.2 Reactor Building Plan View at Elevation 0 m (left) and 3.6 m (right)

For the seismic fragility task, the open-source software OpenSees [4], integrated with the STKO [5] interface, was used. Given that shear walls are the primary structural component responsible for resisting horizontal loads, specifically seismic forces in this context, the multilayer shell element was employed to accurately model the nonlinear response of the structure. This method has demonstrated its effectiveness in capturing the nonlinear behavior of shear walls, as previously validated in the literature, for example references [6–8]. This approach models the different materials within the wall cross-section, such as concrete and steel, as distinct layers, as illustrated in Figure 1.3. The thickness of the steel layers is calculated based on the steel reinforcement ratio within the concrete.

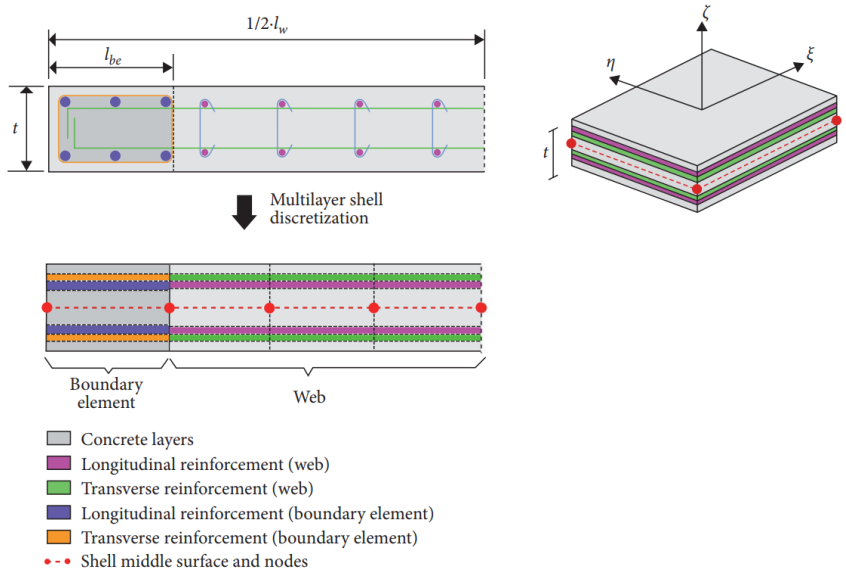

Figure 1.3 RC Shear Wall Modeling Using Multilayer Shell Element [7]

To accurately capture the hysteresis behavior of both concrete and steel, the materials from the OpenSees library were used. Specifically, the DamageTC3D material model, which represents the 3D behavior of concrete, and the Steel02 model for steel were employed. The corresponding stress-strain relationships are illustrated in the following figures:

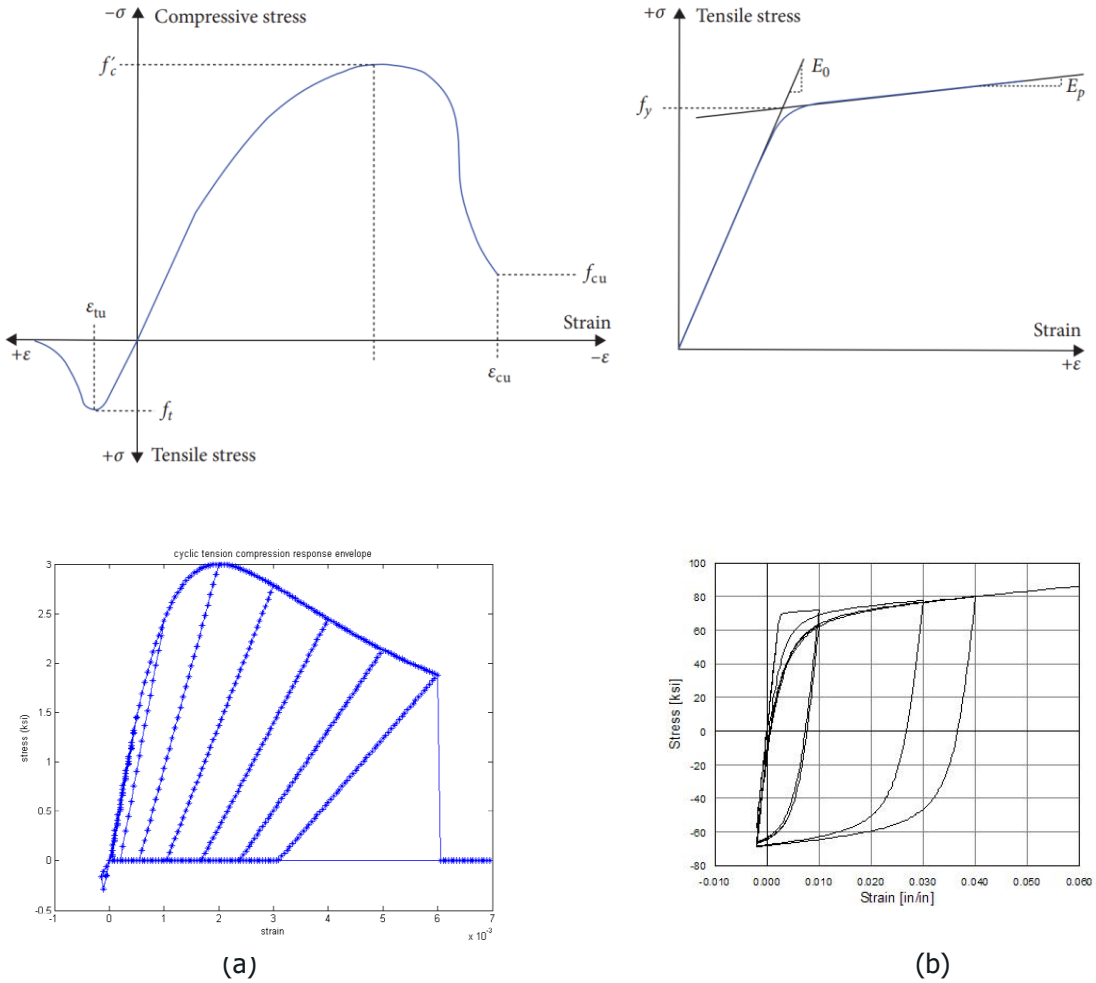

Figure 1.4 Schematic Uniaxial Stress–Strain Curve of the Adopted Material Models: (a) Concrete Model; (b) Steel Reinforcement Model [7]

As previously mentioned in this section, the reactor building includes prestressing tendons within the containment structure. To accurately represent this effect, specific materials and elements were utilized: the Initial Stress Material was applied to introduce stress in the elements, and the fiber section was employed to model the tendons [9].

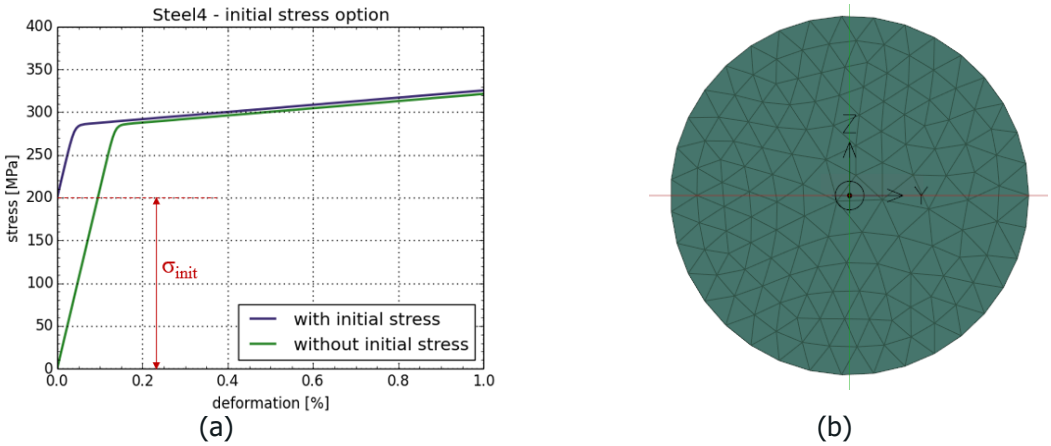

Figure 1.5 (a) Effect of Initial Stress (b) Tendons Fiber Section

The following figure compares the modelling of tendons between the numerical model and Zaporizhzhia NPP reactor building:

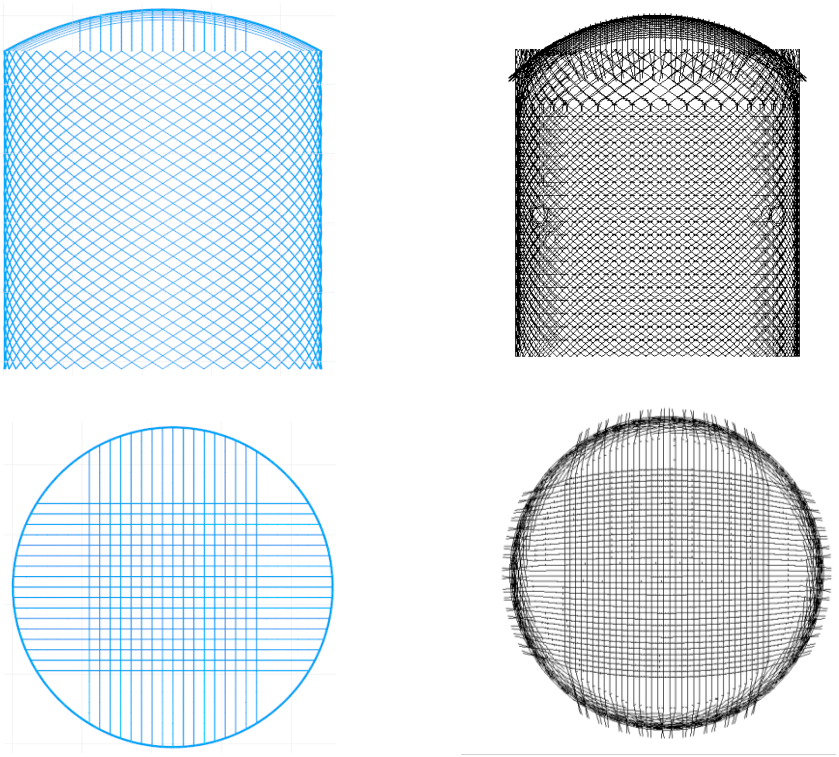

(a) (b)

Figure 1.6 (a) Tendons in the FE Model (b) Tendons in the Reactor Building

The Mechanical properties of the concrete used in this study are given in Table 1.2.

Table 1.2 Materials Properties of the Reactor Building

Material	Density (kg/m^3)	Young's Modulus (MPa)	Poisson's Ratio	Stress (MPa)
Concrete 01	2800	17000	0.2	fc=25
Concrete 02	2800	50000	0.2	fc=25
Reinforcement	7850	200000	0.3	fy=500
Steel cable	/	190000	/	fyp=1335
InitStressMat	/	/	/	σp0=624 (Initial

By integrating all the gathered information and numerical modelling approaches, a numerical model with 145.000 DOF was developed:

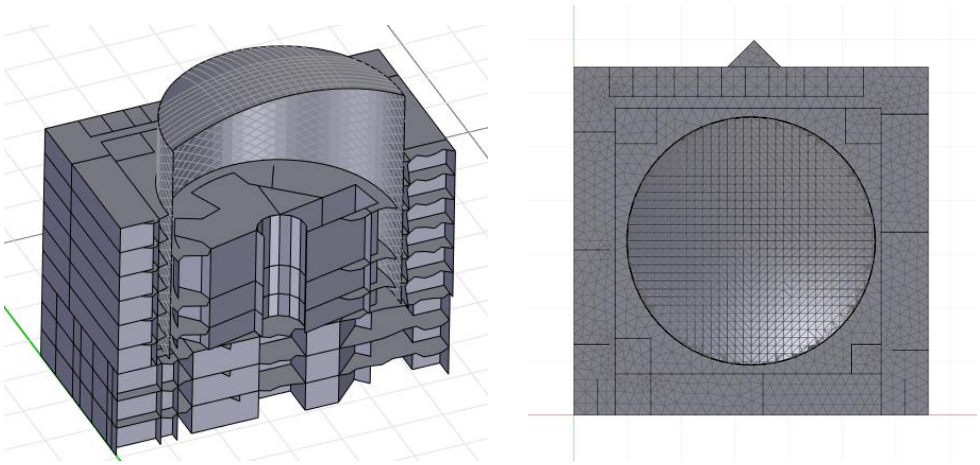

(a) (b)

Figure 1.7 (a) Finite Element (FE) Model of the Reactor Building with Detailed Internal Structures (b) Top View of the Reactor Building's FE model

1.2.2 Diesel Generator Building

The Diesel Generator building of Unit No.1 at the Zaporizhzhia NPP consists of three identical reinforced concrete structures, each housing a diesel generator. 1DGB-1 is in a separate block-cell, while 1DGB-2 and 1DGB-3 share a three block-cell structure (Figures 1.8 and 1.9).

The DGB foundation is a 700 mm thick monolithic reinforced concrete slab made of M200 concrete, with a base elevation of -7.900 m. The external and internal load-bearing walls are constructed using pre-fabricated permanent reinforced concrete formwork. The formwork is 80 mm thick, with overall wall thicknesses of 900 mm (external) and 600 mm (internal). The reinforcements are A I and A III grades, and the concrete is M200 and M300. The floors are prefabricated monolithic slabs made of M200 and M300 concrete, 600 mm thick, with permanent formwork and bottom reinforcement. The channel covers are made of VSt3kp2 steel. The roof slab is also prefabricated monolithic, with a total thickness of 900 mm, reinforced with spatial reinforcement cages. The building is equipped with overhead cranes and hoists.

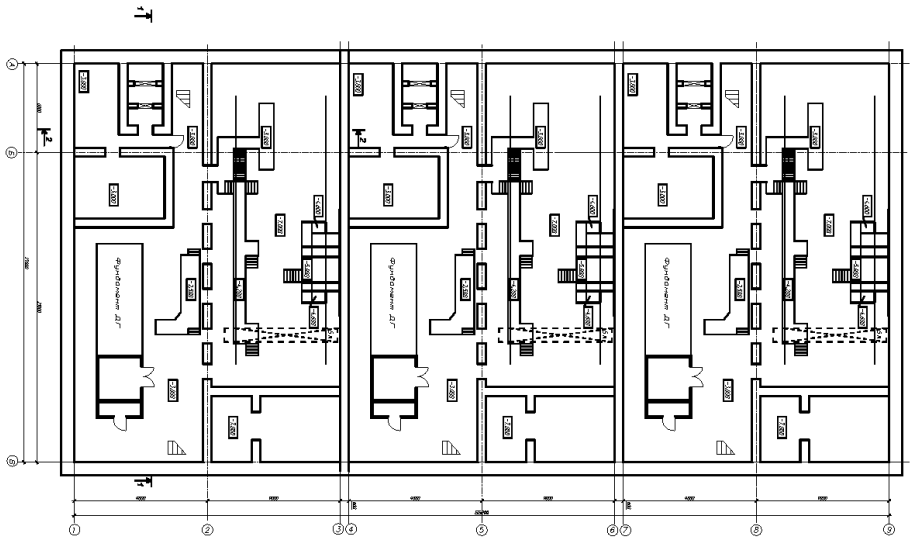

Figure 1.8 Diesel Generator Building (1DGB-2,3) Plan Elevation -3,000 -7,000

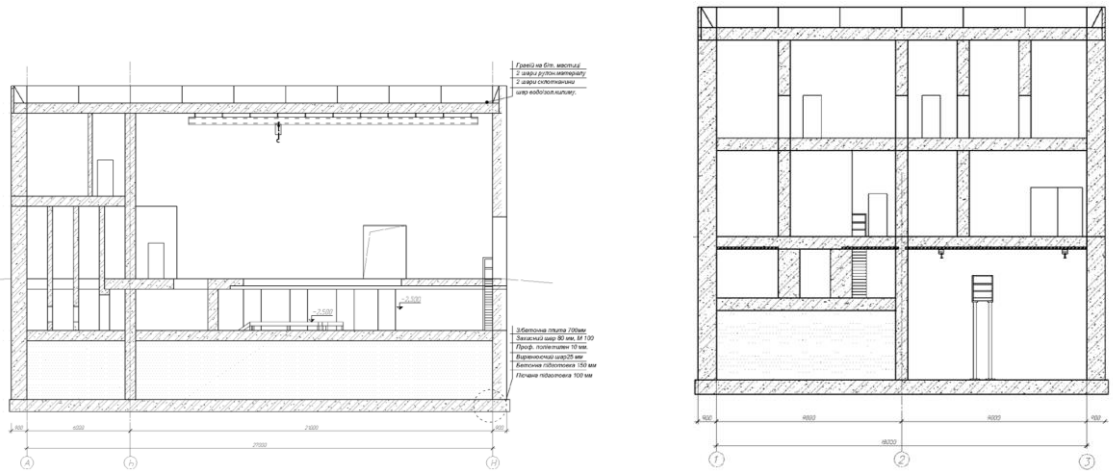

(a) (b)

Figure 1.9 Diesel Generator Building (1DGB): (a) Section Cut 1-1 (b) Section Cut 2-2

To develop a comprehensive numerical model the same modelling options as described for the reactor building (previous section) is used here (Material Nonlinearity, elements type). For the sake of reduced computational effort and since the three DG Buildings are almost identical, only the DGB with reference 1 was developed.

The mechanical characteristics of the materials used for DGB development are presented in Table 1.3. Figure 1.10 shows the 3D finite element model of the reactor building and its inside.

Table 1.3 Materials properties of the DG Building

Material	Density (kg/m^3)	Young's Modulus (MPa)	Poisson's Ratio	Stress (MPa)
Concrete 01	2500	25000	0.2	fc=19
Reinforcement	7850	210000	/	fy=235

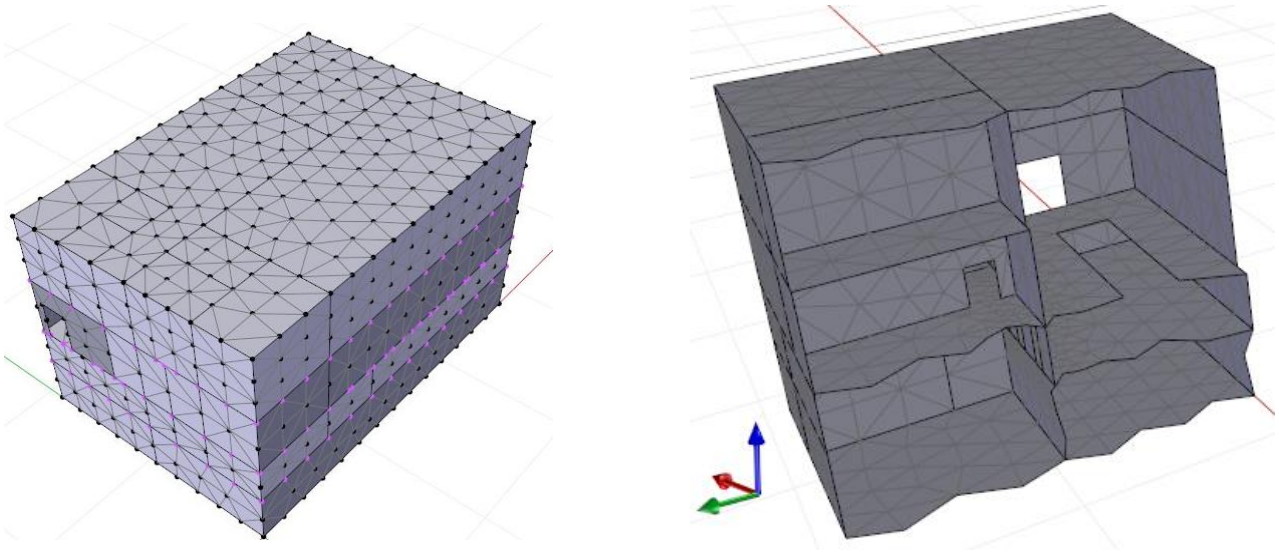

(a) (b)

Figure 1.10 (a) Finite Element (FE) model of the Diesel Generator Building (b) Cross-sectional view of the Diesel Generator Building's FE model

1.2.3 Filter Containment Venting System

One of the critical piping systems in a nuclear power plant is the Filter Venting Containment System [10]. It plays a vital role in preventing overpressure within the reactor's containment structure. However, developing a comprehensive seismic fragility model for this system was challenging due to the limited availability of essential data, such as geometry, cross-section, and support types. To overcome these difficulties, data from an external source from German NPP was utilized. The reference model primarily comprises the dirty gas pipe, venturi scrubber, and clean gas pipe, all constructed from X6CrNiTi18-10 (Nr. 1.4541, Austenitic) material [11]. The structure predominantly uses DN 300.0 profile pipes, with certain sections having different cross-sections. The system also includes insulation for pipe protection, which was accounted for as additional mass distributed in isolated areas. The developed numerical model is shown in Figure 1.11.

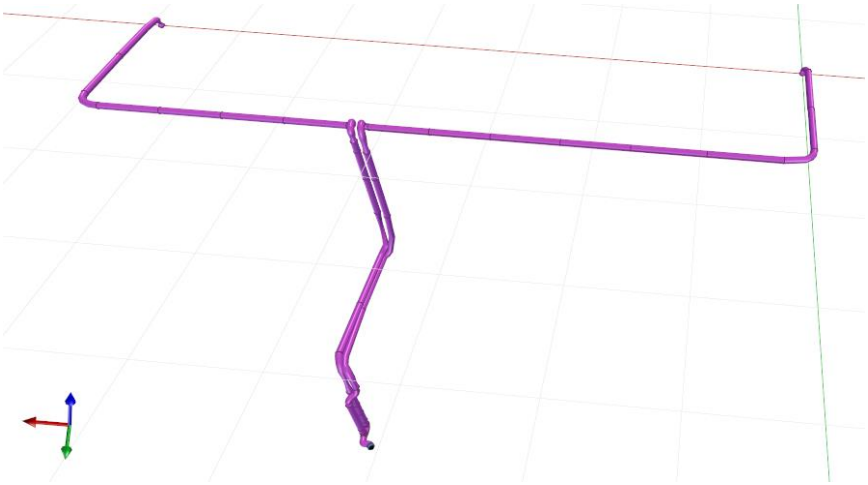

Figure 1.11 FCV System Numerical Model

Since the FCV System passes through different floor levels in the reactor building, different parts of the model are supported by different support condition .Table 1.4 and Figure 1.12 summarize the information on the 31 different supports: supports stiffness, its type and the location of their location within the developed model.

Table 1.4 Supports Types Used in the FCVs System

Support type	Nr.	Stiffness (N/mm)
Fixed point (FP)	3	Fixed
Sliding bearing (GL)	16	2e5
Sliding bearing – GL-X STOP	2	2e5
Sliding bearing with dirs (GLF)	2	2e5
Wall duct (FUE - Ya)	2	2e5
Wall duct (FUE – all sides)	2	2e5
Spring hanger (FH)	4	33.6 and 66.6

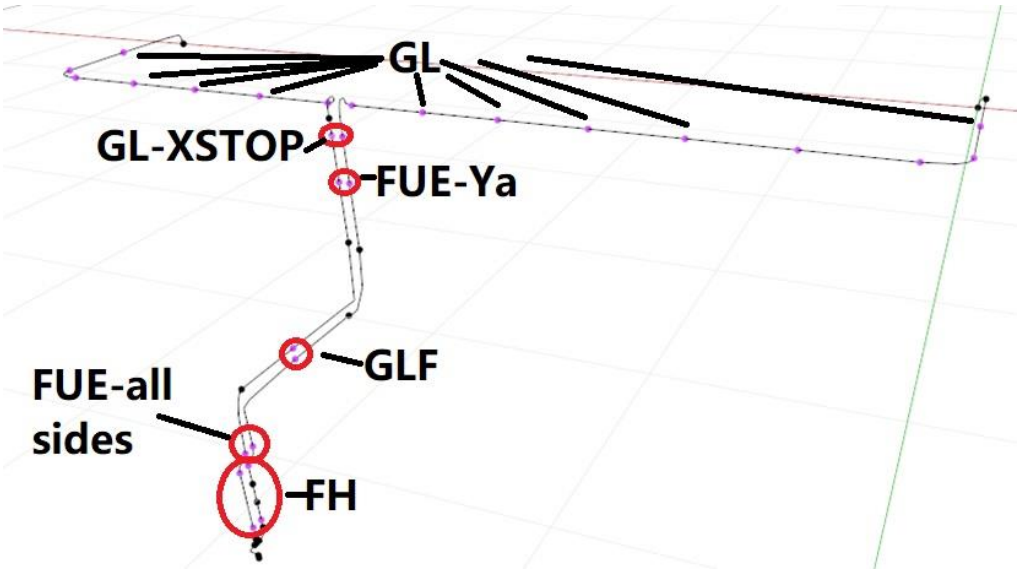

Figure 1.12 Support Locations Within the System

As far as the nonlinear behavior of the system is concerned, the fiber method [9] was utilized on a different section of piping, this is illustrated in Figure 1.13 along with pipe sections in Table 1.5.

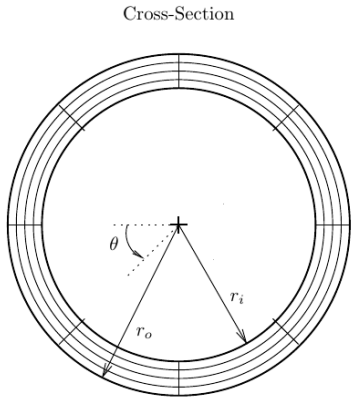

Figure 1.13 Fiber Section of the Piping System

Table 1.5 Cross-Section Dimensions

Profile	Outside diameter D (mm)	thickness t (mm)
DN 300.0	323.9	5.0
DN 300.1	323.9	7.1
DN 300.2	323.9	4.5

1.2.4 Transformer 6kV-380V

One of the key power generation components in the nuclear power plant is the transformer. We consider transformers situated in the reactor building and the diesel generator building. Similar to the FCVs model, the necessary data for developing the numerical model was obtained from external resources [12]. The transformers are clamped and anchored, weighing 2420 kg with a center of gravity at a height of 850 mm. The distance between the clamp's measures 710 mm, and the supporting clamped connection has dimensions of C100x50x8. An example of the component is shown in Figure 1.14

Figure 1.14 Transformer Component located at Zaporizhzhia Nuclear Power Plant (NPP)

The numerical model was developing focusing on capturing the potential failure of the component, as discussed later. To this end, nonlinearity was only modelled in the C100x50x8 elements, which are responsible for carrying both vertical and horizontal loads. The system was simplified to ensure that the forces act in a manner consistent with the expected real behavior, while maintaining the accuracy of the model in representing the critical load-bearing elements. The simplified numerical model is shown in the following figure:

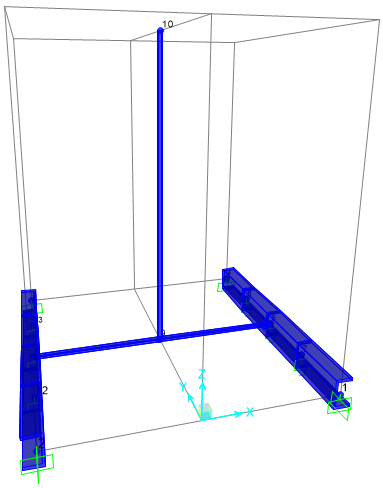

Figure 1.15 Simplified FE model of the Transformer Component

1.2.5 Control Monitor Cabinet

The Control Monitor Cabinet, located in reactor buildings, plays a major role in ensuring and monitoring the safe operation of the reactor. Cabinets are anchored to the floor via expansion anchors and bolted to the cabinet base at the four edges. The cabinet weighs 227 kg, with a center of gravity (CG) positioned at a height of 1125mm. The distance between the clamps used for securing the cabinet is 310mm [12]. The illustration of this component is shown in the following figure:

Figure 1.16 Control Monitor Cabinet located at Zaporizhzhia Nuclear Power Plant (NPP)

In the process of numerical modelling, the focus was on capturing the failure mode of the CMC model. To achieve this, a nonlinear analysis was performed on the anchoring steel angle (40x40x3 mm) to determine its capacity. The characteristics extracted from this analysis were then applied to the properties of the hinges, which were modelled at locations where higher internal forces were anticipated.

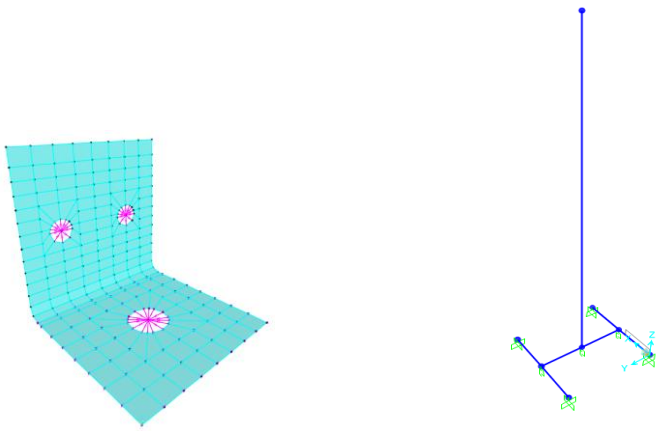

(a) (b)

Figure 1.17 (a) Anchoring Steel Angle (CMC support) (b) Simplified Model for CMC Component

1.2.6 Service Water Pump

The service water pump is a long-column vertical pump anchored to the concrete operating floor of the pump structure using expansion bolts. The properties of the component were assumed to have the same properties as the pump in EPRI report [1] . The complete pump model includes the pump column, pump shaft, motor stand, and motor, all of which were modelled as beam elements (Figure 1.18).

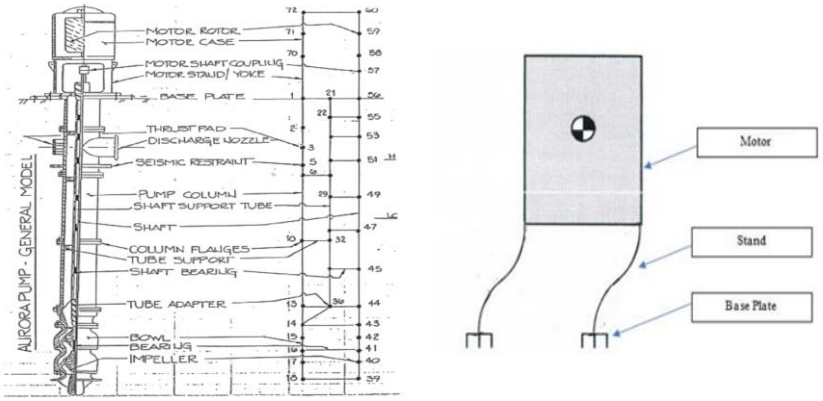

(a) (b)

Figure 1.18 (a) Original Model of the Service Water Pump (b) Simplified Motor Stand Model per EPRI (2018)

The developed simplified model is designed to ensure the capture of the critical failure mode. It is a 3-dimensional stick model featuring an elastoplastic rotational spring at its base, which provides a representation of the failure mode of the water pump motor, identified as the most critical aspect. The simplified model and its expected behavior are illustrated in the following figures:

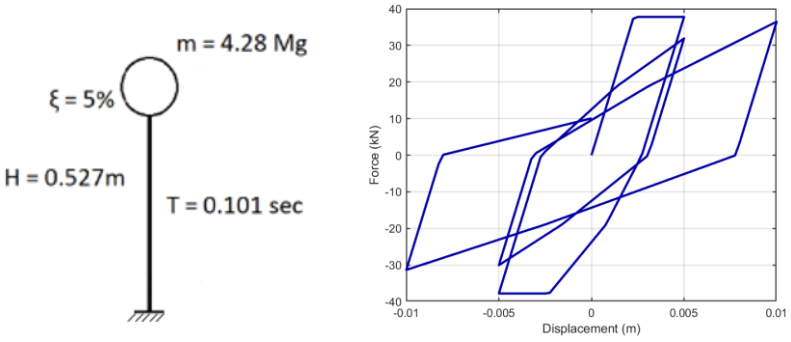

(a) (b)

Figure 1.19 (a) Pump Motor Stand Model (b) Hysteretic Behavior of the Model Under Static Cyclic Loading

The upcoming section will present the validation of these numerical models, specifically focusing on the reactor building model, the diesel generator building model, and the filter venting containment system. The validation is limited to these three models due to their comprehensive and sophisticated modelling nature. The remaining structures were modeled in a simplified manner, which already aligns with the established validation process.

1.3 Numerical Models Validation

During the validation of the numerical models, the modal analysis information related to Zaporizhzhia NPP, along with other resources, was used as a reference for comparison with the modal results obtained from the finite element (FE) models. Additionally, a gravity analysis was conducted to ensure the integrity of the structural elements and to verify the correct assignment of additional masses and vertical loads. This section shows this comparison in terms of structure and system, for the reason of the comprehensive modelling and the necessity of the model verification, as far as the components are concerned, the simplified modelling was performed insuring the capture of modal analysis characteristics.

1.3.1 Reactor Building - FE Model

Eigenvalue analysis of structure is performed to obtain its modal characteristics using the available module in OpenSees (-genBandArpack). Figure 1.20 presents the first six vibration mode shapes and the corresponding natural frequencies of the FE model. It can be noticed that the first two modes are both translational modes x, y with low to medium frequencies, while the remaining have some rotational contribution.

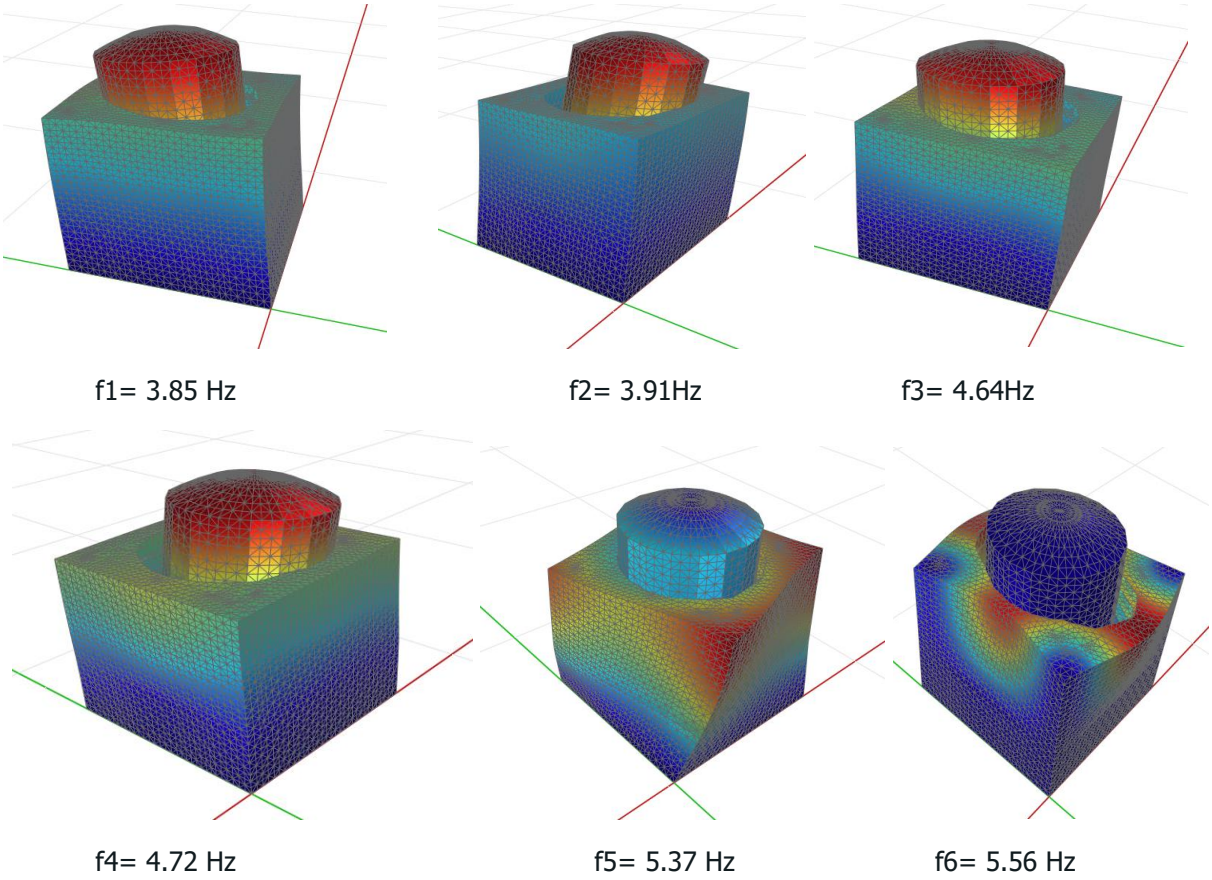

Figure 1.20 Mode Shapes and Natural Frequencies of the Reactor Building FE Model

The final step of the validation process involved comparing the obtained results with the fixed base data of the Zaporizhzhia NPP. This comparison (Table 1.6) demonstrated a good agreement between the numerical model and the reference data, showing less than 5% of deviation in the dominant modes, confirming the accuracy of the model. The modal analysis including the effects of soil-structure interaction (SSI) is presented in the last column. Introducing the soil springs leads to a drop of approximately half in the first frequency compared to the analysis without SSI.

Table 1.6 Comparison of Target and Model Natural Frequencies for the Reactor Building for Modal Validation, with and without SSI

Mode Shapes	Target Frequency (Hz)	FE Model Frequency (Hz)	Variation (%)	Including SSI
1	3.85	3.89	1.04	2.01
2	3.91	4.02	2.81	2.09
3	4.64	4.14	10.78	3.39
4	4.72	4.86	2.97	3.64
5	5.37	5.07	5.59	4.29
6	5.56	5.89	5.94	4.49
7	5.79	6.28	8.46	4.94
8	5.79	6.29	8.64	5.10
9	5.8	6.67	15	5.56
10	5.85	6.95	18.8	5.81

1.3.2 Diesel Generator Building - FE Model

Using the same modal analysis module in OpenSees as employed in the previous section, the first six mode shapes are presented below. When compared to other dynamic characteristics of the NPP structures, the Diesel Generator Building demonstrates a stiff structural response, with modal frequencies ranging from 12 Hz to 28 Hz for the specified mode shapes. In the first two modes, translational behavior predominates, whereas rotational contributions become more significant in the subsequent modes.

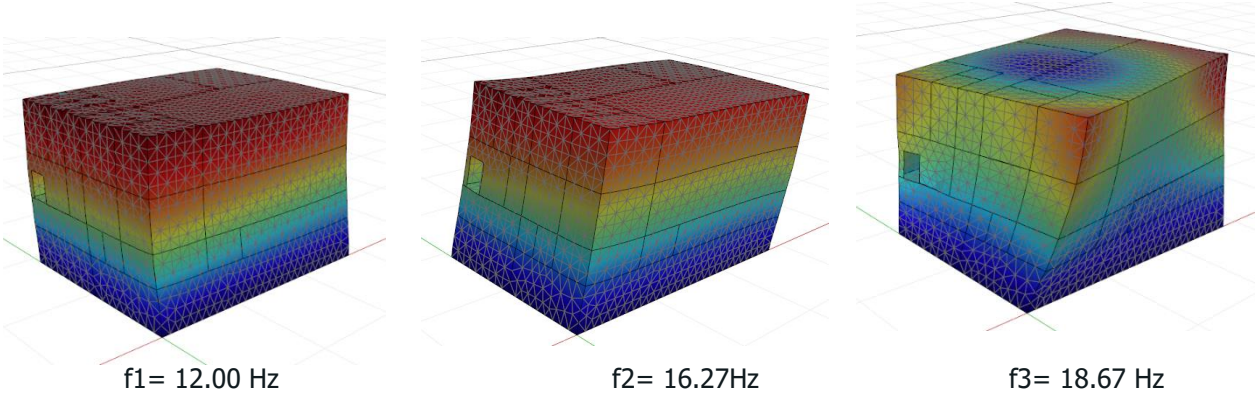

f1= 12.00 Hz f2= 16.27Hz f3= 18.67 Hz

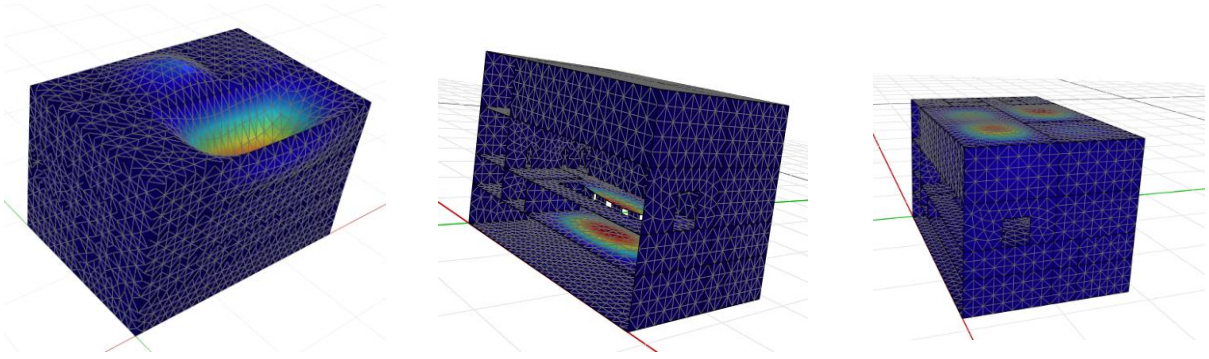

f4= 26.35 Hz f5= 28.19 Hz f6= 28.88 Hz

Figure 1.21 Mode Shapes and Natural Frequencies of the Diesel Generator Building FE Model

The comparison between the obtained modal analysis results and Zaporizhzhia NPP data is presented in Table 1.7, including the influence of soil-structure interaction (SSI). The finite element (FE) model's modal analysis accurately captured the target eigenfrequencies from the reference Zaporizhzhia NPP, with a discrepancy of less than 5% for the dominant modes. The impact of SSI, which is expected to reduce the system's frequencies, is evident in the table, showing a decrease of approximately 30% in the first mode frequency.

Table 1.7 Comparison of Target and Model Natural Frequencies for the DG Building for Modal Validation, with and without SSI

Mode Shapes	Target Frequency (Hz)	FE Model Frequency (Hz)	Variation (%)	Includ-ing SSI
1	12.06	12.00	0.48	8.45
2	16.57	16.27	1.79	9.69
3	17.43	18.67	7.10	13.55
4	19.15	26.35	37.59	16.43
5	19.8	28.19	42.38	24.61
6	20.45	28.88	41.23	26.22
7	21.38	30.76	43.86	27.70
8	21.57	32.73	51.74	28.47
9	22.58	34.61	53.28	29.29
10	23.45	36.09	53.90	29.39

1.3.3 Filter Containment Venting System - FE Model

In contrast to the diesel generator building, the filter containment venting system is considered the most flexible structure compared to other SSCs. This is primarily due to the large dimensions of the system. The frequencies for this system range from 0.957 Hz in the first mode to 4.404 Hz in the sixth mode, as illustrated in the figure below.

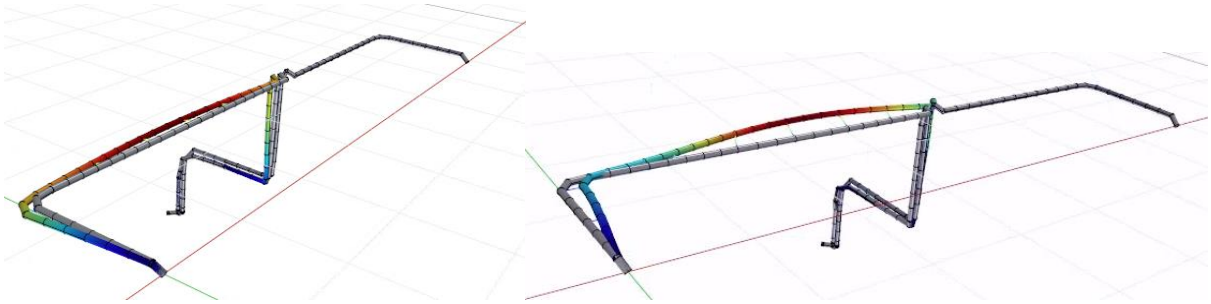

f1= 0.957 Hz

f2= 1.349 Hz

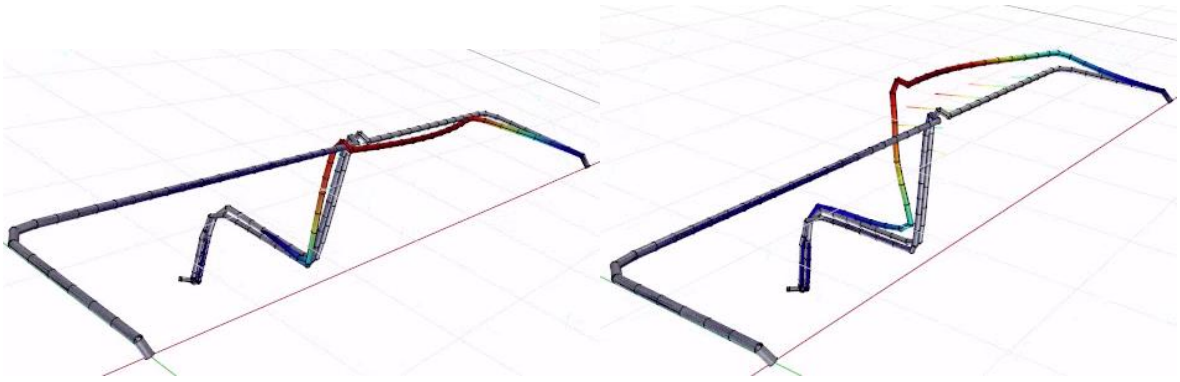

f3= 1.691 Hz f4= 2.576 Hz

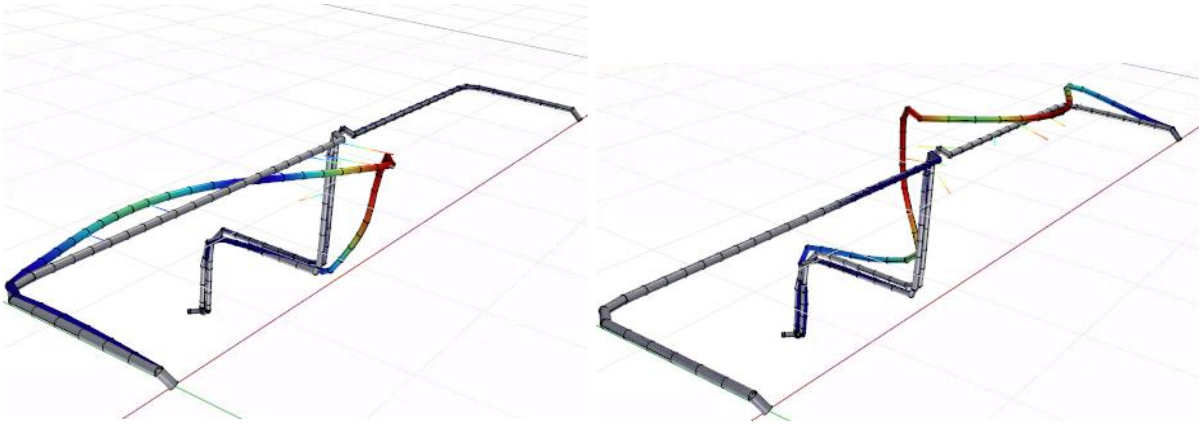

f5= 3.172 Hz f6= 4.404Hz

Figure 1.22 Mode Shapes and Natural Frequencies of the Filter Containment Venting System

Comparing the modal results with the German NPP report [10], the FE model demonstrates a good agreement in capturing the first mode shapes. However, considerable discrepancies are observed in higher modes. These deviations can be primarily attributed to modelling assumptions made in the absence of complete data, such as the characteristics of the support system and other relevant parameters.

Table 1.8 Comparison of Target and Model Natural Frequencies for the FCVs Model for Modal Validation

Mode Shapes	Target Natural Frequency (Hz)	Model Natural Frequency (Hz)	Variation (%)
1	0.93	0.95	2.75
2	1.28	1.34	5.36
3	1.55	1.69	9.01
4	2.21	2.57	16.11
5	2.28	3.17	38.99
6	2.59	4.40	69.59
7	3.05	5.21	70.39
8	4.04	5.24	29.75
9	4.29	5.79	34.86
10	5.14	8.18	59.25

2 Metis Case Study Site and Ground Motion Record Selection

Both finite element (FE) structural models (Reactor Building and Diesel Generator Building) were theoretically situated in Tuscany, Italy. Ground motions developed in the previous work package (WP5) were used to represent the site-specific conditions (more details in METIS D5.4).

These ground motions from WP5 are organized into ten distinct intensity measure levels (IMLs), each corresponding to a different return period. For the site response analysis, five of these IMLs (5, 6, 7, 8, and 9) were considered for SSCs' fragility computations (Table 2.1). In addition to the ground motion variability, uncertainties in the properties of soil profiles were accounted for when conducting the site response analysis to obtain site-specific soil surface ground motion. The final results of WP5 are classified into two main categories: BE (Best Estimate) and BEU (Best Estimate with Uncertainties), representing ground motion at the surface level with and without consideration of uncertainties on site properties, respectively (Figure 2.1).

Table 2.1 IML values for different return periods

IMLs	5	6	7	8	9
Return Period	2500	5000	10000	20000	50000
IM*=PGA (g)	0.132	0.191	0.27	0.377	0.565

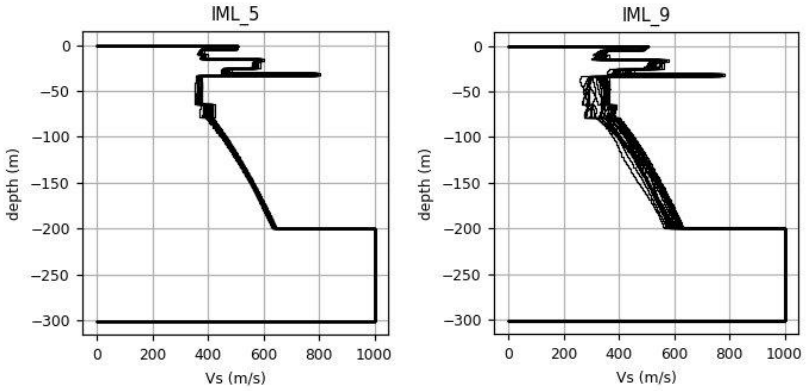

(a)

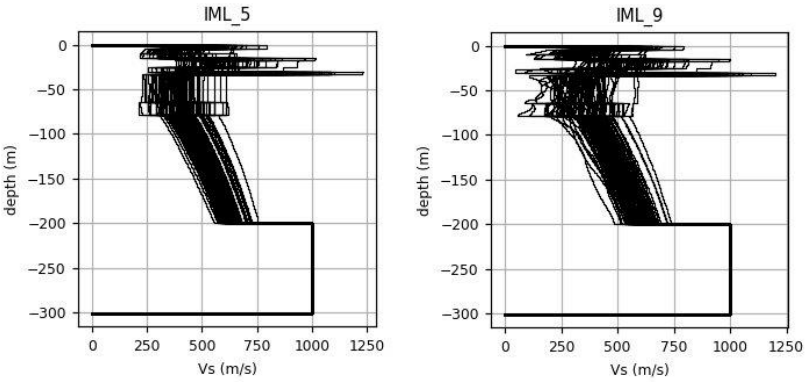

(b)

Figure 2.1 Shear Wave Velocity (Vs) Profile for two IML 5 and 9: (a) Best Estimate (b) Best Estimate with Uncertainties

It is important to note that the developed numerical models, with refined mesh sizes, contain a large number of degrees of freedom (DOFs), resulting in high computational costs. For this reason, the ground motions used in the fragility assessment of the METIS case study models were limited to the last three intensity measure levels (IMLs 7, 8, and 9) for the BEU case, resulting in a total of 250 GMs (50 from IML 7, and 100 each from IMLs 8 and 9). This ensures that uncertainties are adequately accounted for while also including high-intensity ground motions, which allow for the exploration of the structural response under more extreme loading conditions.

3 Fragility Analysis Approach

Fragility analysis is a crucial component of the risk assessment process, as it quantifies the conditional probability that a structure will exceed a specified threshold given a particular hazard level. Various approaches are available in literature to conduct fragility analysis. One approach is Cloud Analysis, which involves generating a "cloud" of data points through numerous nonlinear dynamic analyses, with each point representing a different seismic event and the corresponding structural response [13]. Another widely used method is Incremental Dynamic Analysis (IDA), where structures are subjected to a series of ground motion records scaled to increasing intensity levels to assess their seismic performance [14]. Additionally, Multiple-Stripe Analysis (MSA) evaluates structural performance by analysing responses to ground motion records at different pre-selected or scaled intensity levels, referred to as "stripes," differing from IDA, which uses incrementally scaled motions [15].

As far as nuclear power plants are concerned, Multiple-Stripe Analysis (MSA) faces significant limitations in fragility analysis. The high median capacities of SSCs (Structures, Systems, and Components) in these facilities often result in few, if any, observable failures within the MSA stripes, making it challenging to derive accurate fragility parameters. This is particularly problematic in realistic scenarios, where seismic demands usually fall below the failure threshold, reducing the effectiveness of MSA. Also, the limited number of results per stripe affects the robustness of the failure probability estimations per stripe. On the other hand, the IDA approach seems to be a suitable method for this task because it enables us to explore the structural behavior under extreme loading, but with a high computational cost.

In contrast, the cloud regression method [16] offers a more practical and reliable approach for nuclear applications. It allows for useful visualization of structural behavior as a function of ground motion intensity and extrapolation to higher values, even when there is limited failure data, making it feasible to generate meaningful fragility estimates. By utilizing a lognormal model, the regression method effectively handles the high-capacity values typical in nuclear systems, ensuring that the analysis remains both accurate and applicable. This makes the cloud regression method a more robust and suitable tool for fragility analysis in the nuclear industry, especially when compared to the challenges associated with MSA. For this reason, the cloud regression method is used as the basis for the fragility analysis in this report.

The cloud regression method utilizes nonlinear time history analysis to create a data sample for fragility curve evaluation. This involves representing the seismic load with a set of N triplets of ground motion histories tailored to the site-specific seismic hazard [16]. In conjunction with the regression method, Latin Hypercube Sampling is employed to account for variability at the structural level, including factors such as strength, stiffness, and damping, as well as soil parameters like stiffness and damping in the soil model. This approach effectively propagates uncertainty through the mechanical model and optimizes the exploration of the entire space of possible parameter values.

The regression method requires a sample of N input-output pairs, (α_i, y_i) , i=1,….,N , where the input is the ground motion indicator or seismic intensity level α_i (such as PGA) and the output is the continuous damage measure y_i, The continuous damage measure variable Y is modelled as lognormal random variable :

$$Y = b\,\alpha^{c}\eta \qquad (Eq.1)$$

where η is a lognormal random variable with a median of 1 and a logarithmic standard deviation σ. It is assumed that the structure fails or reaches a certain damage level when the variable Y exceeds a threshold D_S such that $P_f(\alpha)=P(Y>D_S|\alpha)$. The parameters b, c, and σ can be conveniently determined by linear regression in log-space:

$$\ln Y = \ln b + c\ln\alpha + \sigma\varepsilon \qquad (Eq.2)$$

where $\sigma\varepsilon = \ln\eta$, is a centered normal random variable with standard deviation σ, the latter is obtained as the standard deviation (std) of the regression error. Moreover, defining $D_s=bA_m^c$, we have:

$$A_m = \exp\left(\frac{\ln\left(\frac{Ds}{b}\right)}{c}\right) \qquad (Eq.3)$$

In consequence, the fragility curve is described by a lognormal distribution with a median equal to the seismic capacity Am and the lognormal standard deviation $\beta=\sigma/c$ such that:

$$p_f(\alpha) = \Phi\left(\frac{c\,\ln\left(\frac{\alpha}{A_m}\right)}{\sigma}\right) = \Phi\left(\frac{\ln\left(\frac{\alpha}{A_m}\right)}{\sigma/c}\right) \qquad (Eq.4)$$

One key advantage of the linear regression approach is its ability to be utilized even when no or few failures are observed. It doesn't inherently require the scaling of accelerograms and remains effective, even with smaller sample sizes. Although linear regression can be applied to any dataset, it does involve extrapolating the behavior in cases where no failures are observed.

3.1 Reactor Building Model Fragility

To accurately assess the failure probability of structural components, it is essential to examine the seismic response of the structure in which these components are situated. The reactor building is one of the most critical, if not the most critical, structure in nuclear facilities due to the significance of the components it contains. The reactor building, typically characterized by a medium-frequency response (Table 1.6), consists of three primary elements: the containment structure, the outer building, and the foundation (Figure 1.1). To take into consideration soil-structure interaction, the widely recognized methodology of distributed springs was employed to model the soil response for each degree of freedom, which proved its efficiency with respect to the other rigorous methods [17]. The spring and dashpot parameters were calculated based on guidelines provided in the FEMA code [18]. The following tables summarize the input values for the springs and dashpots along with coefficient of variation (COV).

Table 3.1 Stiffness Characteristics of Soil Springs for the Reactor Building Model (Median Values and Standard Deviation) Based on the Considered IML

	IML 7		IML 8		IML 9	
	Median	COV	Median	COV	Median	COV
Horizontal x (N/m)	5.86E+10	0.347	5.50E+10	0.353	4.96E+10	0.416
Horizontal y (N/m)	5.86E+10	0.347	5.50E+10	0.353	4.96E+10	0.416
Vertical z (N/m)	7.98E+10	0.363	7.47E+10	0.371	6.70E+10	0.438
Rotation about the x axis (N·m/rad)	6.45E+13	0.399	6.01E+13	0.408	5.34E+13	0.481
Rotation about the y axis (N·m/rad)	6.45E+13	0.399	6.01E+13	0.408	5.34E+13	0.481
Torsion (N·m/rad)	7.40E+13	0.387	6.90E+13	0.394	6.17E+13	0.462

Table 3.2 Damping Characteristics of Soil Springs for the Reactor Building Model (Median Values and Standard Deviation) Based on the Considered IML

	IML 7		IML 8		IML 9	
	Median	COV	Median	COV	Median	COV
Horizontal x (N.s/m)	3.88E+09	0.187	3.87E+09	0.189	3.66E+09	0.235
Horizontal y (N.s/m)	3.88E+09	0.187	3.87E+09	0.189	3.66E+09	0.235
Vertical z (N.s/m)	9.37E+09	0.163	9.29E+09	0.164	8.93E+09	0.199
About the x axis (N.s/m)	2.14E+12	0.157	2.13E+12	0.162	2.17E+12	0.166
About the y axis (N.s/m)	2.14E+12	0.157	2.13E+12	0.162	2.17E+12	0.166
About the z axis (N.s/m)	2.17E+12	0.188	2.18E+12	0.192	2.25E+12	0.206

To account for the effect of uncertainties propagation, uncertainties in both the structure and the soil were considered. For the structure, uncertainties were included in the yielding point, maximum concrete compressive and tensile strengths, concrete elastic modulus, steel yield strength, steel elastic modulus, and structural damping. For the soil, uncertainties were addressed in each of the defined stiffness and damping parameters, which were calculated based on different soil profiles (Figure 3.1). A lognormal distribution [1,19] was assumed for the structural uncertainties, with the following standard deviations [20]:

Table 3.3 Uncertainties Incorporated into the Reactor Building Model

Properties	logarithmic standard deviation
Concrete Elastic Modulus	0.15
Maximum Compressive Concrete Strength	0.12
Maximum Tensile Strength	0.13
Steel Yielding Strength	0.11
Steel Elastic Modulus	0.15
Damping	0.30

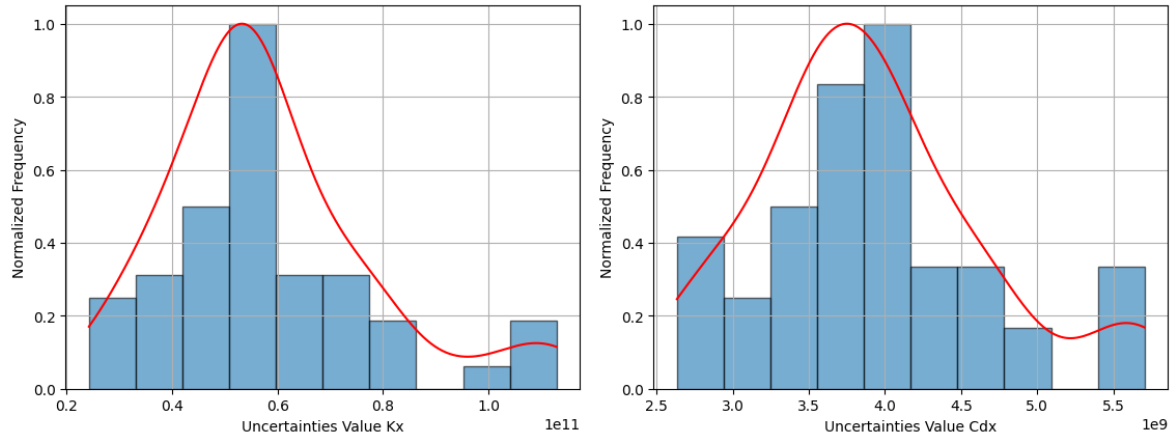

(a) (b)

Figure 3.1 Examples of Uncertainties included in Soil Calculations from soil profile IML8: Histograms and empirical density for (a) Horizontal Stiffness and (b) Horizontal Soil Damping

To define the threshold for fragility analysis, it is important to identify the most critical structural component to study. According to design codes for nuclear power plants, the reactor containment is the most critical part of the reactor building structure [21–24] . This was evaluated by analysing the non-linear behavior under horizontal and gravity loadings (pushover analysis) [25,26], with the lateral forces distributed according to the dominant mode shape pattern. This behavior is shown in the following figure:

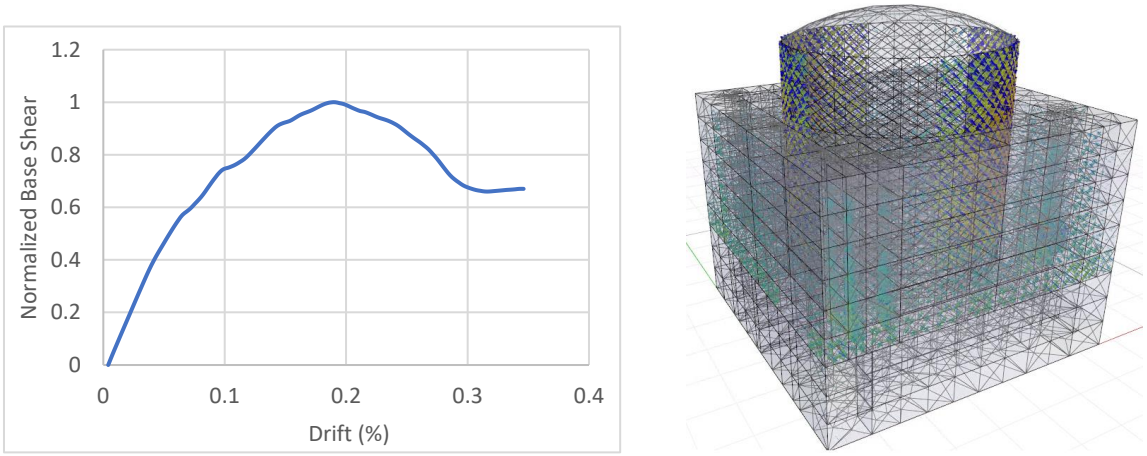

(a) (b)

Figure 3.2 (a) Pushover Curve for Reactor Building (b) Strain Distribution at the Final Stage of Pushover Analysis

The results of the pushover analysis revealed that strain and stress concentrations occurred first in the reactor building containment, followed by the outer building. Consequently, the threshold for the reactor building was defined as the point where the maximum compressive strength was exceeded [21], leading to concrete crushing. Figure 3.3 illustrates the strain development at the stage where concrete failure occurred at the base of the reactor containment. This failure was estimated to occur at a drift of 0.08% of the total height of the containment structure.

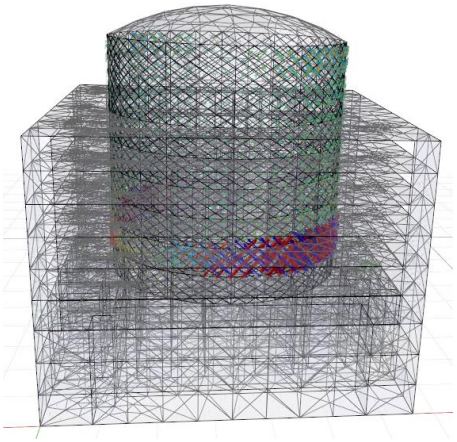

Figure 3.3 Deformation of Reactor Building at Initial Exceedance of Maximum Compressive Strength

Regarding the nonlinear time history analysis, it is important to note that due to the complexity and detail of the modelling, running the analysis with a set of 250 ground motion records would be highly time-consuming. Therefore, a study was conducted to determine the optimal mesh size for accurately capturing the results (by comparing a smaller mesh size with a more refined one).

In this study, the damage index was chosen to be the drift of the containment (top node) combined using the geometric mean definition as illustrated in the Eq.5. This engineering demand parameter (EDP) already demonstrated its effectiveness in accurately capturing the structural response [14,27–29].

$$GeoMean\ Drift = \sqrt{D_x . D_y} \qquad (Eq.5)$$

For the definition of the intensity measure (IM), the peak ground acceleration (PGA) was selected and combined using the geometric mean approach as the engineering demand parameter (EDP). The PGA has demonstrated great efficiency compared to other intensity measures [30–36]. The nominal spectral acceleration used is defined based on the following formula[1]:

$$GeoMean\ PGA = \sqrt{PGA_x . PGA_y} \qquad (Eq.6)$$

Given this definition of Engineering Demand Parameter (EDP) and Intensity Measure (IM) and based on the cloud regression fragility methodology discussed in Section 3, the following Figure 3.4 illustrates the relationship between the IM and EDP:

[1] For METIS case study the hazard and record selection has been performed for rotd50 and not geomean of horizontal ground motion components. For simplicity's sake, here we work with geomean instead which generally close to rotd50.

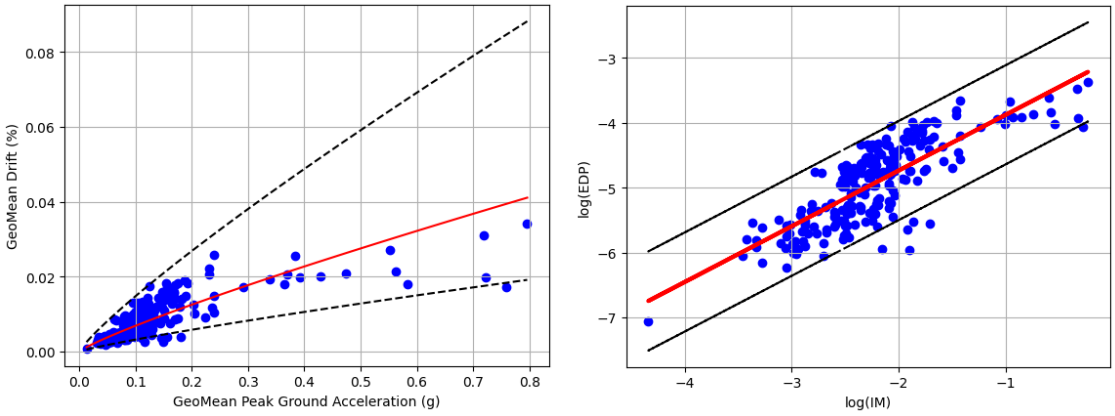

(a) (b)

Figure 3.4 (a) Reactor Building Response Versus Peak Ground Acceleration (PGA) (b) Logarithmic Relationship Between Engineering Demand Parameter (EDP) and Intensity Measure (IM)

Each blue dot in Figure 3.4(a) represents the results of a single nonlinear time history analysis, accounting for uncertainties in structural parameters (Table 3.3), soil properties (Tables 3.1 and 3.2), and site response. After establishing the relationship between the Intensity Measure (IM) and the Engineering Demand Parameter (EDP) through nonlinear history analysis, linear regression in the logarithmic space (Figure 3.4 (b)) was applied to determine the parameters required for deriving the fragility curve elements, namely the median and dispersion.

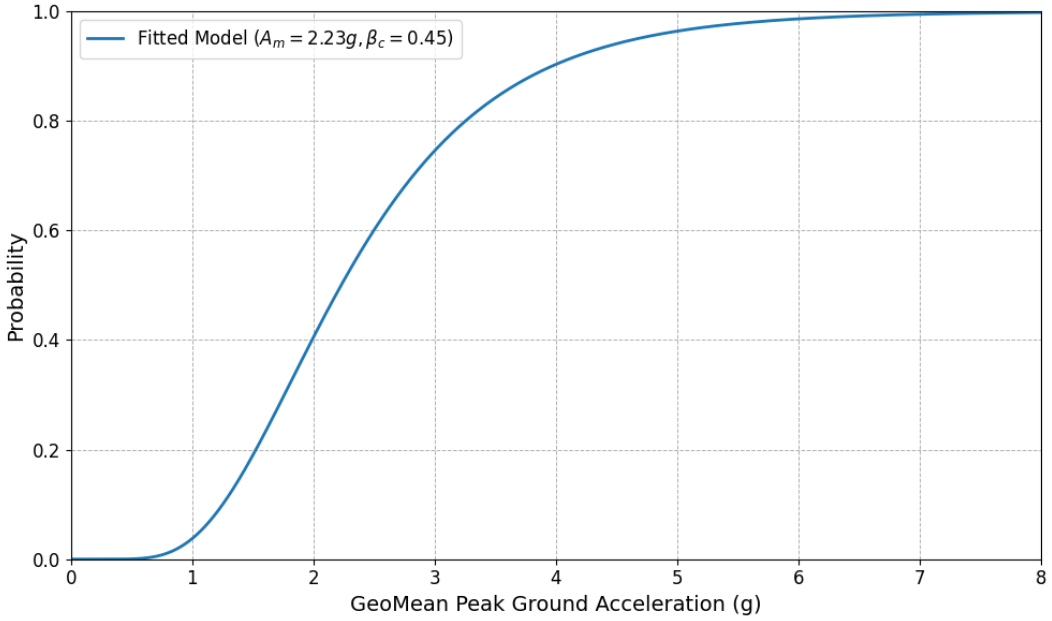

Figure 3.5 Fragility Curve of the Reactor Building Structure

3.2 Diesel Generator Building Model Fragility

As discussed in Section 1.1.2, the diesel generator building is primarily constructed with thick shear walls, resulting in high dynamic characteristics, with the first six mode shapes exhibiting frequencies ranging from 12 Hz to 28 Hz (Figure 1.21). To account for the effect of soil-structure interaction on the response of the diesel generator building, a simplified approach was employed. This approach involved modelling distributed springs at the base of the structure, representing the stiffness and damping properties of the underlying soil. The values for these springs were calculated based on the guidelines provided in FEMA [18] .

Table 3.4 Stiffness Characteristics of Soil Springs for the Diesel Generator Building Model (Median Values and Standard Deviation) Based on the Considered IML

	IML 7		**IML 8**		**IML 9**	
	Median	COV	Median	COV	Median	COV
Horizontal x (N/m)	1.94E+10	0.407	1.82E+10	0.430	1.74E+10	0.445
Horizontal y (N/m)	2.00E+10	0.407	1.88E+10	0.430	1.80E+10	0.445
Vertical z (N/m)	1.98E+10	0.495	1.83E+10	0.527	1.74E+10	0.542
Rotation about the x axis (N·m/rad)	1.55E+12	0.520	1.44E+12	0.551	1.36E+12	0.568
Rotation about the y axis (N·m/rad)	2.68E+12	0.491	2.48E+12	0.519	2.37E+12	0.532
Torsion (N·m/rad)	2.89E+12	0.435	2.70E+12	0.459	2.59E+12	0.474

Table 3.5 Damping Characteristics of Soil Springs for the Diesel Generator Building Model (Median Values and Standard Deviation) Based on the Considered IML

	IML 7		**IML 8**		**IML 9**	
	Median	COV	Median	COV	Median	COV
Horizontal x (N.s/m)	4.29E+08	0.192	4.17E+08	0.200	4.02E+08	0.221
Horizontal y (N.s/m)	4.30E+08	0.192	4.18E+08	0.200	4.04E+08	0.221
Vertical z (N.s/m)	1.43E+09	0.123	1.40E+09	0.127	1.37E+09	0.144
Rotation about the x axis (N.s/m)	3.82E+10	0.049	3.85E+10	0.051	3.85E+10	0.073
Rotation about the y axis (N.s/m)	1.16E+11	0.079	1.15E+11	0.084	1.14E+11	0.109
Torsion (N.s/m)	5.59E+10	0.143	5.51E+10	0.149	5.43E+10	0.171

To accurately propagate uncertainties to the SSCs response, uncertainties were accounted for both in the structure and the soil. For the structure, uncertainties were considered in the yielding point, maximum concrete compressive and tensile strengths, concrete elastic modulus, steel yield strength, steel elastic modulus, and structural damping. For the soil, uncertainties were considered in each of the defined stiffness and damping parameters (Table 3.4 and 3.5) and were derived from each soil profile. The probability distributions of the structural uncertainties were assumed to be lognormal [1]. The following table summarizes the logarithmic standard deviations associated with the selected uncertainties:

Table 3.6 Uncertainties Incorporated into the Diesel Generator Building Model

Properties	logarithmic standard deviation
Concrete Elastic Modulus	0.15
Maximum Compressive Concrete Strength	0.12
Maximum Tensile Strength	0.13
Steel Yielding Strength	0.11
Steel Elastic Modulus	0.15
Damping	0.30

To conduct the fragility analysis, it is essential to define the threshold, which represents the limit state at which the structure is considered to have failed. To accurately establish the limit state for the diesel generator building, a pushover analysis combined with a gravity analysis was performed. This static approach provides insights into both the linear and nonlinear performance of the building under applied loads. The applied loading pattern was specifically designed to align with the building's dominant mode shape. The resulting pushover curve (Figure 3.7 (a)) illustrates the relationship between the normalized base shear and the roof drift.

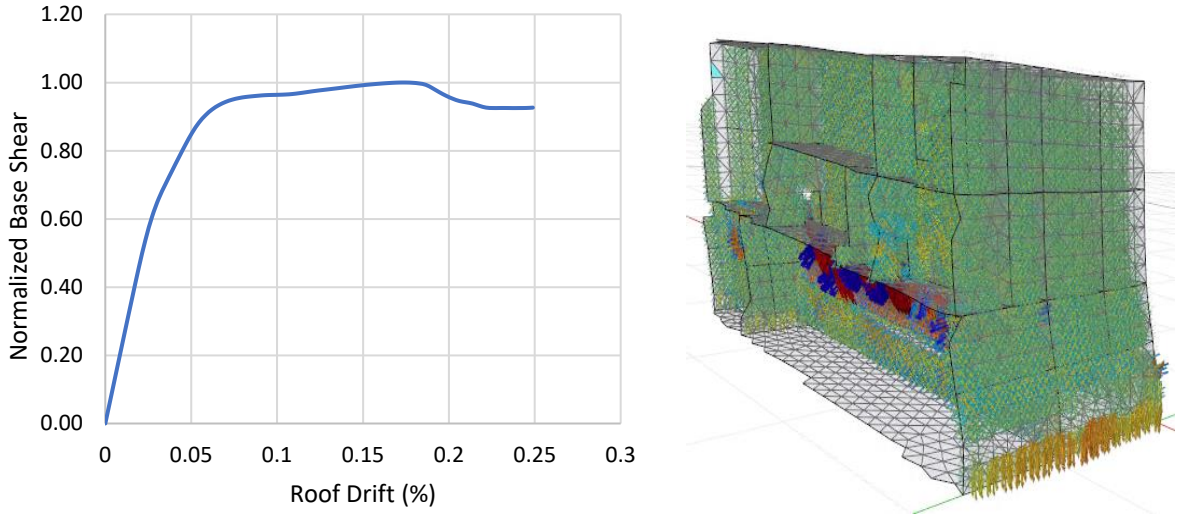

(a) (b)

Figure 3.6 (a) Pushover Curve for Diesel Generator Building (b) Strain Distribution at the Final Stage of Pushover Analysis

Given that the building's horizontal resistance relies on shear walls (both interior and exterior in each direction), the structure is considered to experience local failure when the applied stresses in the interior shear walls reaches the maximum compressive strength of the concrete [37]. This is expected to occur at roof drift ratio of 0.04%.

After conducting the nonlinear time history analysis, the relationship between the IM and EDP of the DGB response is illustrated in Figure 3.8 (a), from where the parameter of the DGB-fragility was derived. It is important to note that the NLTHA results from DGB show more outliers compared to the RBM results. This is mainly due to uncertainties in damping (low values), which lead to an amplification of the response.

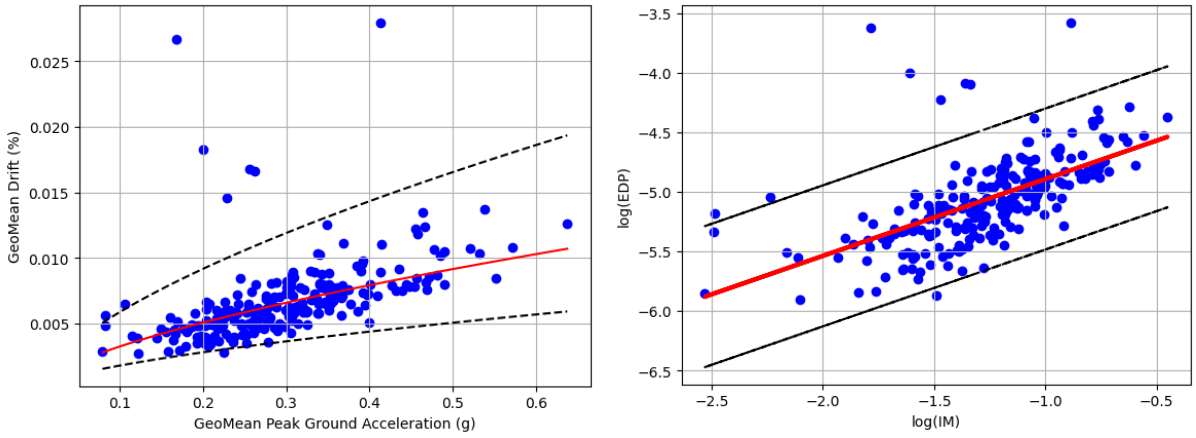

(a) (b)

Figure 3.7 (a) Diesel Generator Building Response Versus Peak Ground Acceleration (PGA) (b) Logarithmic Relationship Between Engineering Demand Parameter (EDP) and Intensity Measure (IM)

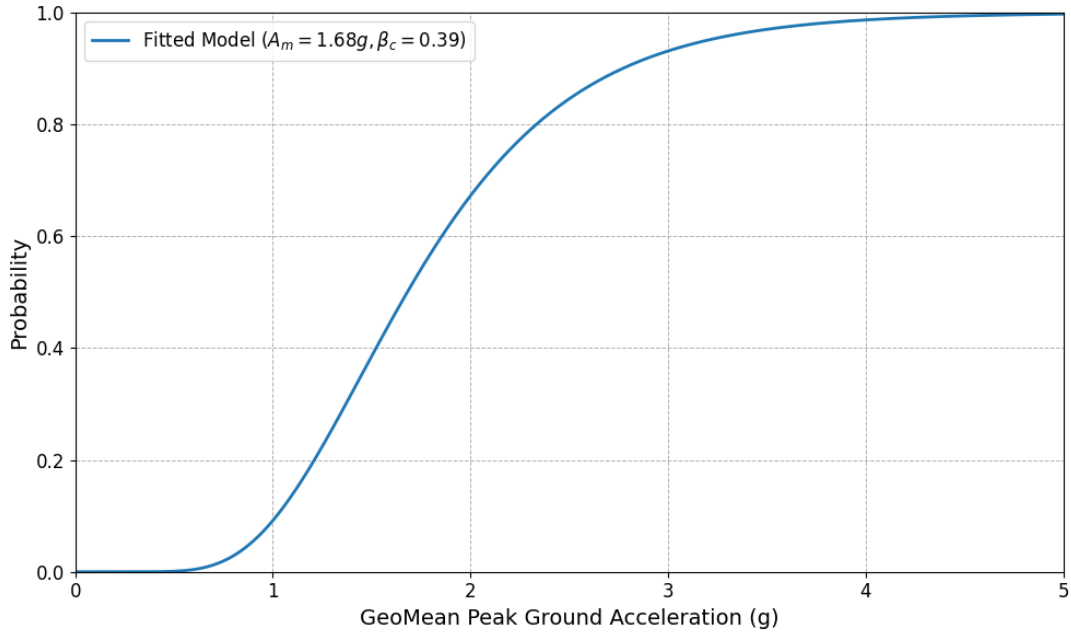

Figure 3.8 Fragility Curve of the Diesel Generator Building

3.3 Filter Containment Venting System Model Fragility

The filtered containment venting system (FCVs), located within the reactor building, is classified as a soft structure based on the modal analysis results (Figure 1.22), in comparison to other components studied in this report. The time history analysis for the FCVs presents a challenge, as the model spans multiple floor levels within the reactor building. This requires extracting time history responses from several floors of the reactor building model to serve as input excitations for the system.

The different support locations of the FCVs model within the reactor building are outlined in the table below:

Table 3.7 Location of FCV Model Supports within the Reactor Building

Support type	location
Fixed point (FP) / Sliding bearing (GL)	45.6 m
Fixed point (FP)	13.2 m
Wall duct (FUE - Ya)	36.6 m
Sliding bearing with dirt (GLF)/ Sliding bearing – GL-X STOP	29.4 m
Wall duct (FUE – all sides) / Spring hanger (FH)	19.2 m

Uncertainties in the elastic modulus and strength of the pipe steel, and structural damping were accounted for. The standard deviations of the assumed lognormal distribution for these uncertainties are 0.13, 0.15, and 0.17, respectively [10].

The failure of a piping system is typically defined either by the failure of the supports (such as FUE-Ya, GLF, etc.) or by the failure of the pipe itself when it exceeds a predefined strain threshold [38]. In this analysis, the second failure mode was considered, where the pipe is deemed to fail if the developed strain exceeds 0.2%. To identify the most critical element that exhibits this deformation first, a series of analyses were performed using time history data in the x, y, and z directions. The results revealed that element-106 near the lower base support (node 78) was the first to exhibit the critical deformation, as shown in the following figure:

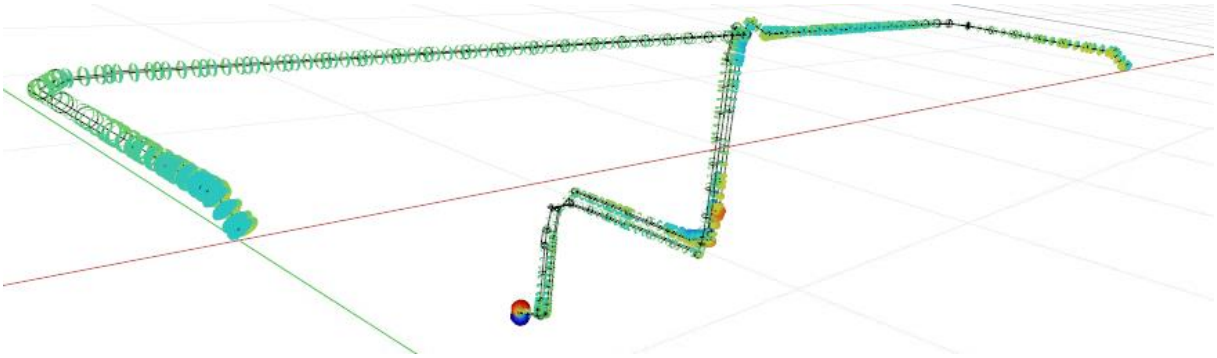

Figure 3.9 Example of Developed Strain in FCV system under the 3D excitation

After identifying the failure modes of the studied piping system, the displacement of the base node was selected as a damage indicator for the fragility analysis. It is expected that the developed strain will reach the critical threshold when the support point undergoes a deformation of 0.1 meters.

After extracting the reactor building responses at the floor levels shown in Table 3.7, dynamic nonlinear analyses were conducted. Figure 3.11 shows the strain developed at the critical element 106. Although the system exhibited nonlinear behavior, the element of interest did not reach the defined strain threshold of 0.2%.

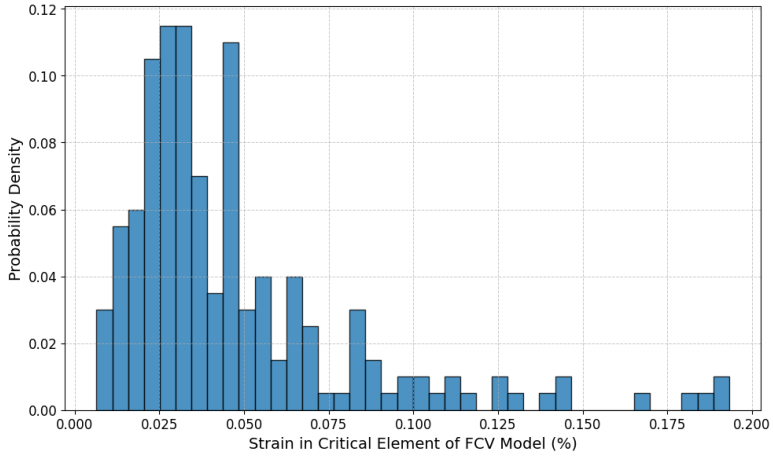

Figure 3.10 Strain Distribution in FCVs-Element 106 from Time History Analysis

The resultant responses from the multi-support three-directional time history analysis are illustrated in the figure below, alongside the corresponding fragility curve.

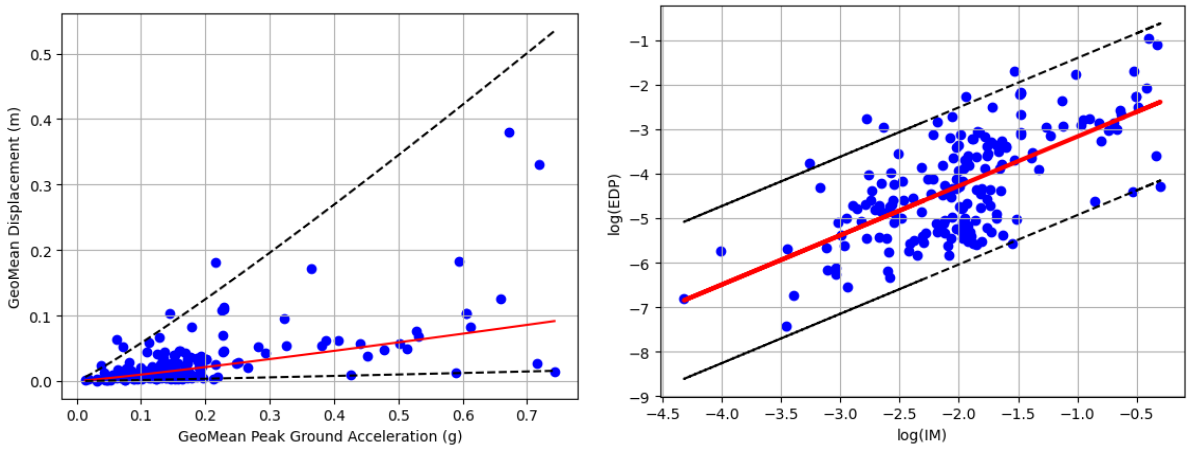

(a) (b)

Figure 3.11 (a) Filter Venting Containment System Response Versus Peak Ground Acceleration (PGA), (b) Logarithmic Relationship Between Engineering Demand Parameter (EDP) and Intensity Measure (IM)

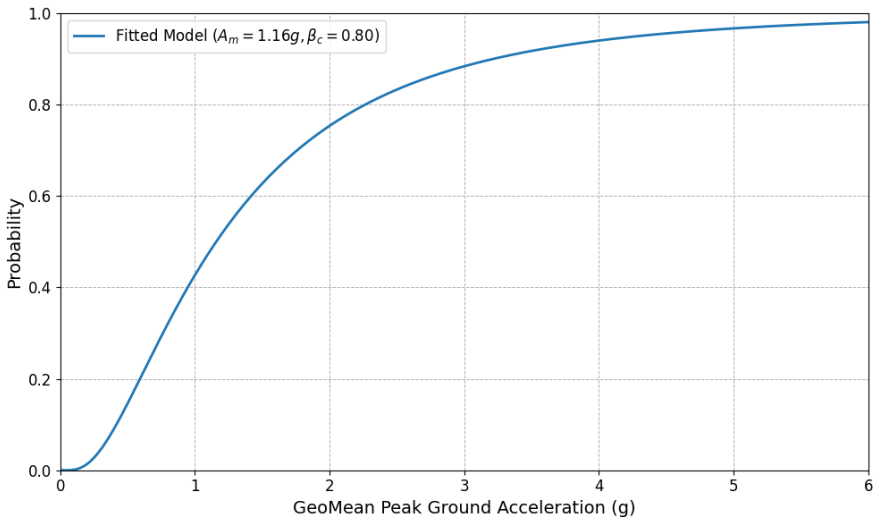

Figure 3.12 Fragility Curve of the Filter Containment Venting System

3.4 Transformer Model Fragilities

3.4.1 Assessment of Transformer Model Fragility Within Reactor Building

We first consider a transformer model located in the reactor building. This simplified transformer model has a natural frequency of 7.5 Hz, accurately reflecting the characteristics of the on-site transformer. The floor response at an elevation of 20.4 m, corresponding to the transformer's location within the reactor building, was utilized as input for the seismic fragility study. Transformer failure was defined by the failure of the supporting elements, specifically the extended C-section with dimensions C100x50x8, subjected to combined loading. To capture the nonlinear behavior of the C-section, it was modelled using a fiber section approach. Following a moment-curvature analysis and the combination of forces from different directions, the component's failure was estimated to occur at a displacement of 0.01 m.

The uncertainties in the transformer model were considered in terms of the capacity of the C-section, damping, and the fundamental period, with values 0.21, 0.18, and 0.15 respectively [12].

After extracting the response at the location of interest and conducting the nonlinear time history analysis, the performance of the transformer component is shown in the figure below:

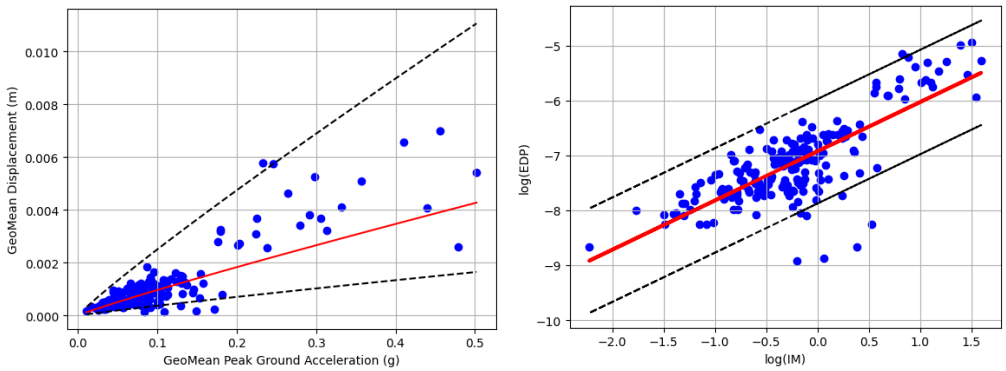

(a) (b)

Figure 3.13 (a) RB-Transformer Response Versus Peak Ground Acceleration (PGA), (b) Logarithmic Relationship Between Engineering Demand Parameter (EDP) and Intensity Measure (IM)

After defining the threshold, the failure probability of the transformer component was determined using the same method described earlier.

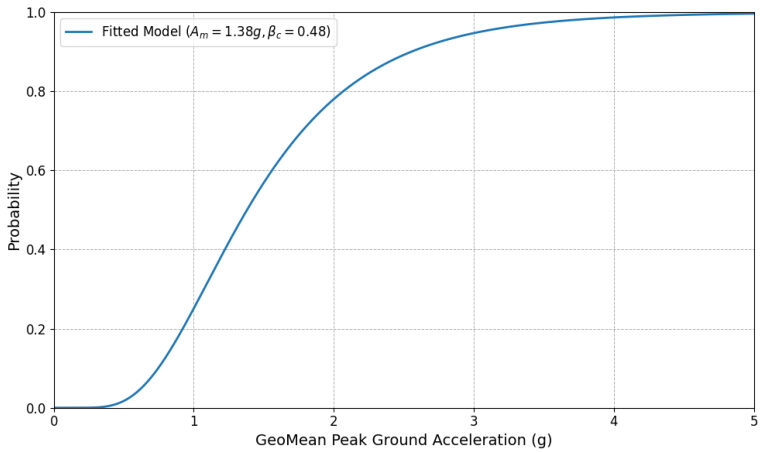

Figure 3.14 Fragility Curve of Transformer located in Reactor Building

3.4.2 Assessment of Transformer Model Fragility Within DG Building

The second transformer considered here is located in the diesel generator building at elevation level 0. As with the previous model, the floor response at this location was extracted and used as input to analyse the seismic response of the transformer model. This transformer model shares the same dynamic characteristics and structural capacity as the model previously discussed. The same values for input uncertainties and threshold definitions, as previously established, were applied in this analysis. The component response based on the input from the diesel generator building is presented below:

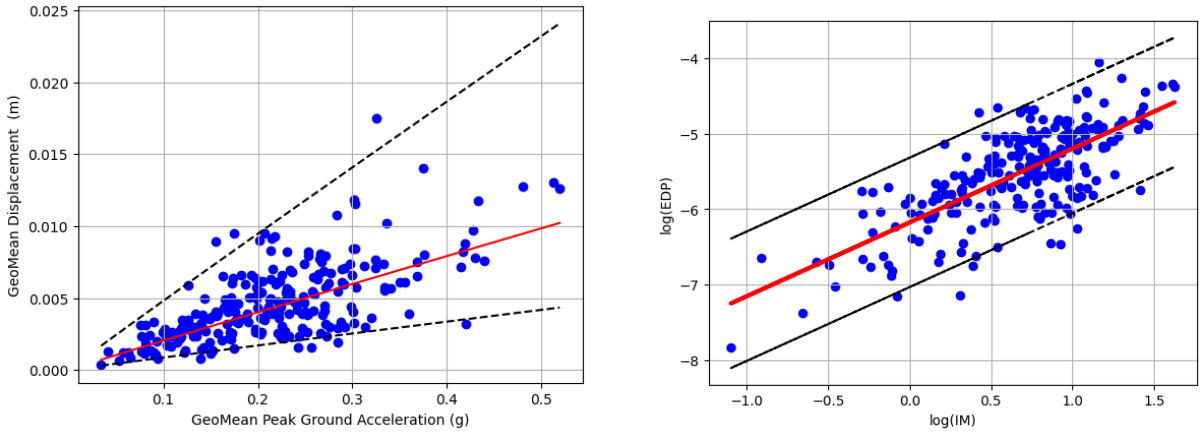

(a) (b)

Figure 3.15 (a) DGB-Transformer Response Versus Peak Ground Acceleration (PGA) (b) Logarithmic Relationship Between Engineering Demand Parameter (EDP) and Intensity Measure (IM)

As previously outlined in this section, the cloud regression method was employed to estimate both the median and the dispersion related to the specified failure of the component.

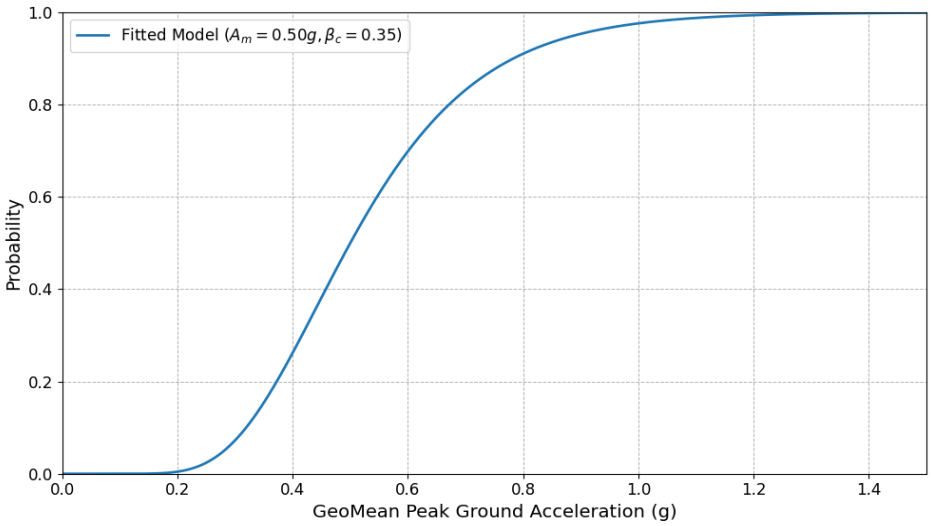

Figure 3.16 Fragility Curve of Transformer located in Diesel Generator Building

3.5 Control Monitor Cabinet Model Fragility

After conducting the nonlinear time history analysis of the reactor building—specifically focusing on the component located within it, the response at an elevation of 13.2 meters was extracted and used as input to study the component's failure. The simplified model of the CMC, which falls within a medium frequency range of approximately 7.5 Hz, was modelled to accurately capture the failure of the component. In this context, the failure is determined by the failure of the supporting element, specifically the anchoring steel angle (40x40x3 mm). This failure occurs when the anchoring steel angle [39,40] reaches its maximum capacity under combined loading conditions, which is estimated to happen when the component reaches a displacement of 3 mm.

To account for the impact of uncertainties on the structural response, the analysis considered key uncertainties in the main component characteristics, including the horizontal and vertical capacities of the anchoring steel angle, damping, and fundamental period. The uncertainties were modelled using lognormal distribution with the following values: 0.11 for horizontal/vertical capacity, 0.26 for damping, and 0.28 for component period [12].

After performing the analysis, the response of the CMC component is illustrated in the figure below, alongside its fragility curve.

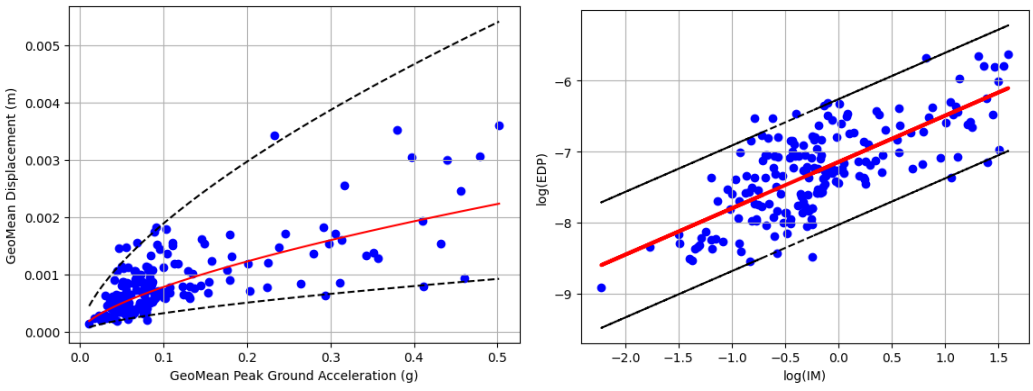

Figure 3.17 (a) Control Monitor Cabinet Response Versus Peak Ground Acceleration (PGA) (b) Logarithmic Relationship Between Engineering Demand Parameter (EDP) and Intensity Measure (IM)

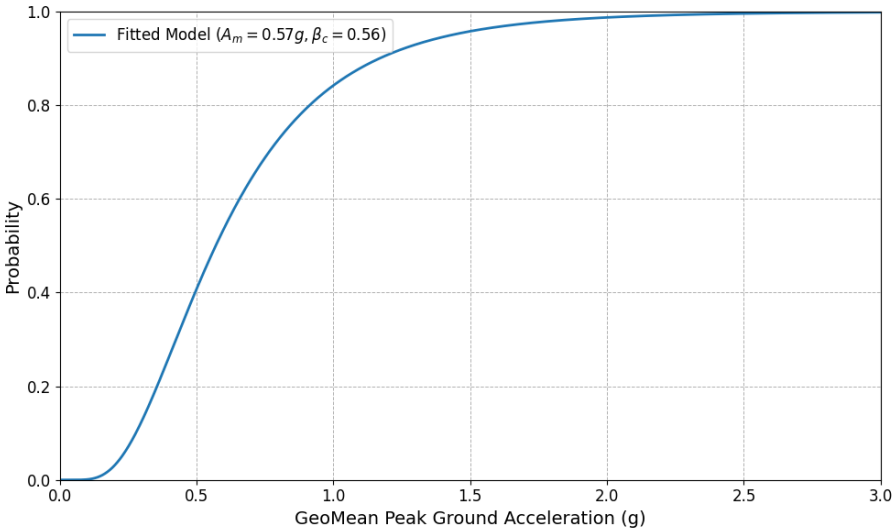

Figure 3.18 Control Monitor Cabinet Fragility Curve

3.6 Service Water Pump Model Fragility

The pump model located in the diesel generator building at elevation -7 was analysed, with the floor response at this specific location extracted and used as input excitation to assess the component's failure probability. The simplified pump model, with a frequency of approximately 9.9 Hz (≈ 10 Hz), is considered to have failed when the pump motor fails (anchorage failure). This failure was estimated to occur at a ductility level of 1.25. Consistent with previously defined components EDP, displacement was used as the damage indicator. Based on information from the EPRI report [1], the component's capacity (V_{yield} = 37.79kNm, M_{yield} = 19.91kN) was used to estimate the displacement at which failure occurs, calculated to be 2.9 mm (Figure 3.20).

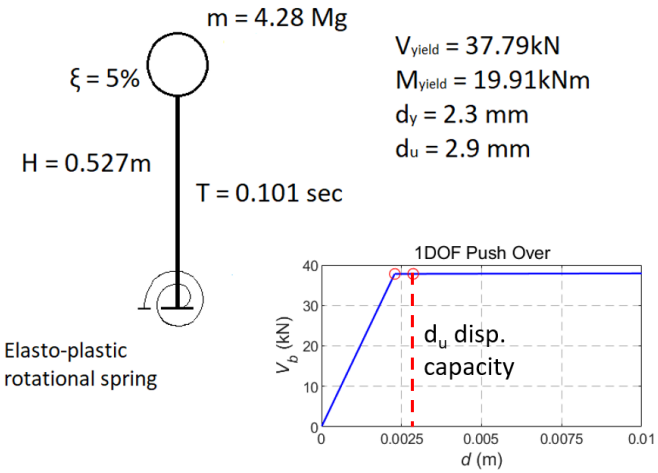

Figure 3.19 Service Water Pump Simplified Model and Threshold Definition

The uncertainties on the structural elements such as the moment capacity of the component, damping and the fundamental time period were considered. The uncertainties were modelled using lognormal distribution with the following values: 0.18 for moment capacity, 0.16 for damping, and 0.12 for time period. Based on these definitions, the three-directional time history analysis was conducted, and the response of the SWP component, along with its fragility curve, is illustrated below.

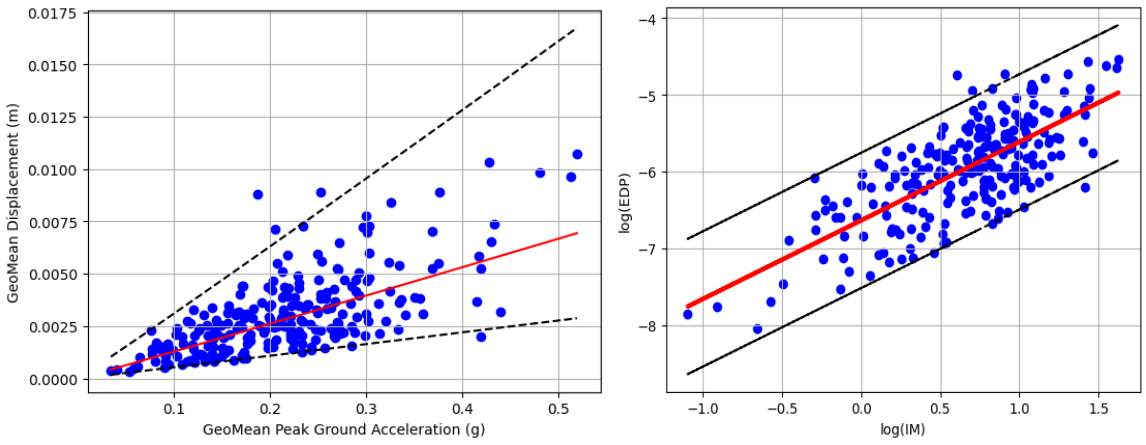

(a) (b)

Figure 3.20 (a) Pump Motor Stand Model Response Versus Peak Ground Acceleration (PGA) (b) Logarithmic Relationship Between Engineering Demand Parameter (EDP) and Intensity Measure (IM)

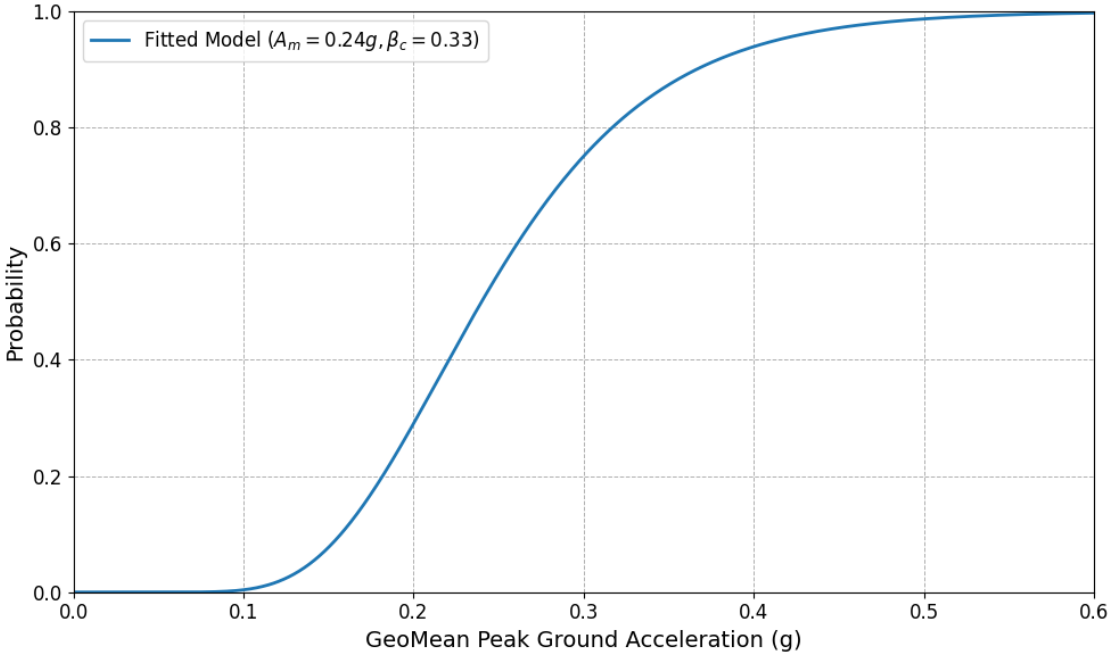

Figure 3.21 Pump Motor Stand Model fragility curve

3.7 Summary of the SSCs Fragility Results

The fragility assessment of the structures, systems, and components (SSCs) under consideration indicates a diverse range of seismic performance. Among the assessed SSCs, the Reactor Building emerges as the most robust structure, exhibiting the highest median seismic capacity. However, it also demonstrates relatively higher variability in its response when compared to the diesel generator building.

Conversely, the Filter Containment Venting System (FCVs) exhibits the highest variability (0.8), attributed to its support being located at different elevations within the reactor building. This multi-support excitation introduces significant uncertainty in its seismic response, as components anchored at varying elevations are subjected to differential seismic forces and motions, in addition to the sensitivity of the system to the vertical excitation.

The remaining components—Transformers, Control Monitor Cabinet (CMC), and Service Water Pump (SWP)—exhibit low to medium median fragility values and moderate variability in seismic response. Among these, the SWP component is the most vulnerable of all the considered Structures, Systems, and Components (SSCs). However, a marked discrepancy has been observed in the fragility-median capacity of the transformers located in the reactor and diesel generator buildings, despite their identical characteristics. This disparity can be attributed to the floor response, as the diesel generator building exhibits a high-frequency response that closely aligns with the transformer's natural frequency, whereas the reactor building has a lower frequency response. The results of the SSCs' fragility parameters are summarized in Table 3.8, alongside the High Confidence Low Probability of Failure (HCLPF) values, calculated using the following formula:

$$HCLPF = A_m \,.\, e^{-2.3\,.\,\beta_c} \qquad (Eq.7)$$

where A_m and β_c are the median capacity (in terms of PGA) and the logarithmic standard deviation (dispersion) respectively.

Table 3.8 Summary of SSCs fragility curves parameters

SSCs	Median Capacity PGA (g)	β_c	HCLPF (g)
Reactor Building	2.23	0.45	0.79
Diesel Generator Building	1.68	0.39	0.69
FCVs	1.16	0.80	0.18
Transformer / RB	1.38	0.48	0.46
Transformer / DGB	0.50	0.35	0.22
Control Monitor Cabinet	0.57	0.56	0.16
Service Water Pump	0.24	0.33	0.11

For comparison purposes, Table 3.9 presents the ZNPP fragility parameters of the selected SSCs and those reported in the EPRI study [41,42]:

Table 3.9 Fragility Data from Various Sources

	ZNPP			EPRI				
				Am (g)			HCLPF (g)	
SSCs	**Am (g)**	**βc**	**HCLPF (g)**	**Ground Level**	**Ad-justed**	**βc**	**Ground Level**	**Ad-justed**
Reactor Build-ing	0.73	0.46	0.25	2.00	/	0.46	0.68	/
Diesel Genera-tor Building	0.91	0.46	0.31	1.50	/	0.46	0.51	/
Transformer /RB	0.97	0.46	0.33	2.00	1.00	0.46	0.68	0.34
Transformer /DGB	1.49	0.46	0.51	1.50	1.50	0.46	0.51	0.51
Control Moni-tor Cabinet	1.17	0.46	0.40	2.00	1.00	0.46	0.68	0.34
Service Water Pump	2.69	0.46	0.92	2.00	2.00	0.46	0.68	0.68
	2.31	0.46	0.79					

4 Conclusions

This deliverable presents the development of six numerical models representing the representative structures and equipment of the Zaporizhzhia Nuclear Power Plant (NPP) using the open-source software OpenSees. Advanced finite element modeling techniques were employed to accurately capture the behavior of these structures. The developed FE models were subsequently validated against data related to the Zaporizhzhia NPP and other relevant NPP studies. Additionally, this report outlines the fragility assessment methodology used to evaluate the probability of failure of the NPP models, incorporating relevant uncertainties and selected ground motions.

The validation process for the FE models against the Zaporizhzhia NPP data and an external report included a gravity analysis to confirm the structural integrity of the models and a modal analysis to ensure they accurately capture the intended dynamic characteristics. The gravity analysis results closely matched the target values, as did the modal analysis outcomes. However, a minor discrepancy of less than 5% was observed in the dominant modes of structures (Reactor Building, Diesel Generator Building, and Filter Containment Venting System) following calibration of the numerical models. It is also noteworthy that this discrepancy increased in higher modes, primarily due to assumptions made where data were insufficient for some modelling parameters.

The results from the fragility analysis (median capacity, dispersion) revealed that the main structural elements, such as the Reactor Building and Diesel Generator Building, exhibit high median capacities with moderate dispersion values (0.45 and 0.39, respectively), indicating strong resistance to seismic forces and relatively low variability in response. In contrast, systems like the Filter Containment Venting System (FCVs) show lower median capacity with a higher dispersion value (0.80), suggesting a greater vulnerability to seismic activity and increased variability in response, this is mainly due to its multi-support configuration at various elevations within the Reactor Building, which introduces additional variability. A notable difference has been observed in the fragilities of the transformers in the reactor building and the diesel generator building, despite their identical characteristics. This was mainly due to the floor response at the location of the component, as the diesel generator building exhibits a high-frequency response that closely aligns with the transformer's natural frequency, whereas the reactor building has a lower frequency response. On the other hand, the most vulnerable component among the selected SSCs was the service water pump.

In summary, this deliverable presents the development and validation of six finite element models of structures and equipment at the Zaporizhzhia Nuclear Power Plant (NPP) using OpenSees, incorporating advanced modelling techniques to replicate structural behavior accurately. Validation against the Zaporizhzhia NPP report and other studies involved gravity and modal analyses, which confirmed structural integrity and accurate dynamic characteristics, with minor discrepancies in dominant modes attributed to modelling assumptions. Fragility analysis results demonstrated that in this case study main structures, such as the Reactor Building and Diesel Generator Building, possess high seismic resistance with moderate response variability. In contrast, systems like the Filter Containment Venting System exhibit greater variability due to their complex support configurations while other components showed moderate resilience.

5 Acknowledgments

Special thanks are extended to the SSTC team for their collaboration in providing the data, despite the challenges. Sincere gratitude is also expressed to the project coordinator Dr. Zentner and the work package leader Dr. V. Alves-Fernandes for their support and cooperation.

6 References

[1] EPRI, Seismic Fragility and Seismic Margin Guidance for Seismic Probabilistic Risk Assessments (2018).
[2] K. Porter, A Beginner's Guide to Earthquake Fragility Vulnerability and Risk (2021).
[3] Oleksandr Sevbo, D6.1 Definition and classification scheme of SSCs for specific and generic seismic fragility evaluation (2021).
[4] McKenna, F., Fenves, G. L, and Scott, M. H., Open System for Earthquake Engineering Simulation.

[5] Asdea, ASDEA software technology, scientific ToolKit for OpenSees, STKO.
[6] Jiang, Lei, Michael W. Chernuka, and Neil G. Pegg., A co-rotational, updated Lagrangian formulation for A co-rotational, updated Lagrangian formulation for geometrically nonlinear finite element analysis of shell structures ((1994)) 129–140.
[7] G. Solorzano, V. Plevris, An Open-Source Framework for Modeling RC Shear Walls Using Deep Neural Networks, Advances in Civil Engineering 2023 (2023) 1–17. https://doi.org/10.1155/2023/7953869.
[8] A. Vatanshenas, Nonlinear Analysis of Reinforced Concrete Shear Walls Using Nonlinear Layered Shell Approach, Nordic Concrete Research 65 (2021) 63–79. https://doi.org/10.2478/ncr-2021-0014.
[9] M. Terrenzi, E. Spacone, G. Camata, 2020. Comparison Between Phenomenological and Fiber-Section Non-linear Models. Front. Built Environ. 6, 38. https://doi.org/10.3389/fbuil.2020.00038.
[10]Technical Report "Fragility Assessment Filter Containment Venting System at German Nuclear Power Plant ".
[11]Mechanical Properties of X6CrNiTi18-10 Material (2018).
[12]Scope of Fragility Evaluation Czech Republic NPP (2008).
[13]J.W. Baker, Efficient analytical fragility function fitting using dynamic structural analysis Earthquake Spectra 31, no. 1 579-599 (2015).
[14]D. Vamvatsikos, C.A. Cornell, Incremental dynamic analysis, Earthq Engng Struct Dyn 31 (2002) 491–514. https://doi.org/10.1002/eqe.141.
[15]J.W. Baker, Conditional Mean Spectrum: Tool for Ground-Motion Selection, J. Struct. Eng. 137 (2011) 322–331. https://doi.org/10.1061/(ASCE)ST.1943-541X.0000215.
[16]I. Zentner, M. Gündel, N. Bonfils, Fragility analysis methods: Review of existing approaches and application, Nuclear Engineering and Design 323 (2017) 245–258. https://doi.org/10.1016/j.nucengdes.2016.12.021.
[17]B. Bapir, L. Abrahamczyk, T. Wichtmann, L.F. Prada-Sarmiento, 2023. Soil-structure interaction: A state-of-the-art review of modeling techniques and studies on seismic response of building structures. Front. Built Environ. 9, 1120351. https://doi.org/10.3389/fbuil.2023.1120351.
[18]Applied Technology Council (ATC) for the Federal Emergency Management Agency, FEMA P-2091, A Practical Guide to Soil-Structure Interaction (2020).
[19]Shinozuka, M, Feng, Lee, J, a. Naganuma, T, Statistical Analysis of Fragility Curves.
[20]J.H. Kim, I.-K. Choi, J.-H. Park, Uncertainty analysis of system fragility for seismic safety evaluation of NPP, Nuclear Engineering and Design 241 (2011) 2570–2579. https://doi.org/10.1016/j.nucengdes.2011.04.031.
[21]L. E. Cover, M. P. Bohn, R. D. Campbell and D. A. Wesley, Handbook of Nuclear Power Plant Seismic Fragilities (1983).
[22]Choi, I.K., Choun, Y.S., Ahn, S.M. and Seo, J.M, Seismic fragility analysis of a CANDU type NPP containment building for near-fault ground motions (2006).

[23]Kanellopoulos Konstantinos, Dynamic Structure-Soil-Structure-Interaction for Nuclear Power Plants.
[24]Choi, Byunghyun, et al, Identification of the reactor building damage mode Identification for seismic fragility assessment using a three-dimensional finite element model (2022).
[25]S. Themelis, PUSHOVER ANALYSIS FOR SEISMIC ASSESSMENT AND DESIGN OF STRUCTURES (2008).
[26]A.M.B. Nafeh, G.J. O'Reilly, Simplified pushover-based seismic risk assessment methodology for existing infilled frame structures, Bull Earthquake Eng 21 (2023) 2337–2368. https://doi.org/10.1007/s10518-022-01600-y.
[27]A. Stocchi, B. Richard, Sensitivity of engineering demand parameters as a function of structural typology and assessment method, Nuclear Engineering and Design 343 (2019) 151–165. https://doi.org/10.1016/j.nucengdes.2019.01.006.
[28]Miranda, E. and Reyes, C., Approximate Lateral Drift Demands in Multistory Buildings with Nonuniform Stiffness (2002).
[29]S. Tesfamariam, K. Goda, Seismic Performance Evaluation Framework Considering Maximum and Residual Inter-Story Drift Ratios: Application to Non-Code Conforming Reinforced Concrete Buildings in Victoria, BC, Canada, Front. Built Environ. 1 (2015). https://doi.org/10.3389/fbuil.2015.00018.
[30]D.-D. Nguyen, T.-H. Lee, V.-T. Phan, Optimal Earthquake Intensity Measures for Probabilistic Seismic Demand Models of Base-Isolated Nuclear Power Plant Structures, Energies 14 (2021) 5163. https://doi.org/10.3390/en14165163.
[31]D.-D. Nguyen, B. Thusa, M.S. Azad, V.-L. Tran, T.-H. Lee, Optimal earthquake intensity measures for probabilistic seismic demand models of ARP1400 reactor containment building, Nuclear Engineering and Technology 53 (2021) 4179–4188. https://doi.org/10.1016/j.net.2021.06.034.
[32]H.D. Nguyen, M. Shin, J.M. LaFave, Optimal intensity measures for probabilistic seismic demand models of steel moment frames, Journal of Building Engineering 65 (2023) 105629. https://doi.org/10.1016/j.jobe.2022.105629.
[33]Z.-K. Huang, K. Pitilakis, S. Argyroudis, G. Tsinidis, D.-M. Zhang, Selection of optimal intensity measures for fragility assessment of circular tunnels in soft soil deposits, Soil Dynamics and Earthquake Engineering 145 (2021) 106724. https://doi.org/10.1016/j.soildyn.2021.106724.
[34]C. Li, C. Zhai, S. Kunnath, D. Ji, Methodology for selection of the most damaging ground motions for nuclear power plant structures, Soil Dynamics and Earthquake Engineering 116 (2019) 345–357. https://doi.org/10.1016/j.soildyn.2018.09.039.
[35]K. Kostinakis, A. Athanatopoulou, K. Morfidis, Correlation between ground motion intensity measures and seismic damage of 3D R/C buildings, Engineering Structures 82 (2015) 151–167. https://doi.org/10.1016/j.engstruct.2014.10.035.
[36]Kramer, S.L. and Stewart, J.P., Geotechnical earthquake engineering (2024).
[37]R. Bustamante, G. Mosqueda, M. Kim, Enhanced Seismic Protection System for an Emergency Diesel Generator Unit, Energies 15 (2022) 1728.

https://doi.org/10.3390/en15051728.
[38]N.E. CSNI, OECD/NEA/CSNI Status Report on Filtered Containment Venting (2014).
[39]T.T. Nahar, M.M. Rahman, D. Kim, Seismic capacity evaluation of fire-damaged cabinet facility in a nuclear power plant, Nuclear Engineering and Technology 53 (2021) 1331–1344. https://doi.org/10.1016/j.net.2020.09.004.
[40]K. Salman, T.-T. Tran, D. Kim, Seismic capacity evaluation of NPP electrical cabinet facility considering grouping effects, Journal of Nuclear Science and Technology 57 (2020) 800–812. https://doi.org/10.1080/00223131.2020.1724206.
[41]EPRI, Updated Equipment Seismic Capacities from Experience Data for Use in the Fragility Calculations. Report 3002011627.
[42]EPRI, Seismic Probabilistic risk assessment implementation guide. Report 1002989, Electric Power Research Institute EPRI, Palo Alto, CA., (2013).